Research Square

Preprints are preliminary reports that have not undergone peer review.
They should not be considered conclusive, used to inform clinical practice,
or referenced by the media as validated information.

Seasonal tick encounters and spatial variation in pathogen prevalence across U.S. NEON sites, 2019–2024

Mansoor Hussain
University of Minnesota
Suhail Ahmed
Khairpur Medical College, Banaras Colony
Benjamin Cull
cull0122@umn.edu

University of Minnesota

Research Article

Keywords: Amblyomma americanum. Ixodes scapularis. Dermacentor variabilis. NEON. tick phenology. tick-borne pathogens. pathogen co-detection. hierarchical models

Posted Date: November 27th, 2026

DOI: https://doi.org/10.21203/rs.3.rs-11776611/v1

License: This work is licensed under a Creative Commons Attribution 4.0 International License. Read Full License

Additional Declarations: No competing interests reported.

Abstract

Longitudinal surveillance can be standardized to allow for the assessment of tick occurrence, abundance conditional on occurrence, and prevalence of pathogens as distinct outcomes. We evaluated 7,667 NEON tick-sampling visits from 2019 to 2024 of adult *Amblyomma americanum*, adult *Dermacentor variabilis* and nymph *Ixodes scapularis*. Seasonal, annual, sampling and weather associations were tested by hierarchical occurrence and zero-truncated count models. Seasonal variation was present in all four groups, with positive abundance. False-discovery-rate corrected weather effects were still important for both stages of *A. americanum*, except for interpretation of the nymphs due to residual spatial autocorrelation. After Benjamini–Hochberg correction, 11 of 20 contrasts were significant, although site-cluster bootstrap intervals often contained the null, suggesting a lack of clarity about interannual differences. The recovery of pathogen tested *A. americanum* nymphs and *I. scapularis* nymphs by exact-visit linkage was 97.9% and 95.2%, respectively. For selected pathogens, interannual variability in prevalence was supported for *Ehrlichia ewingii*. The positive relationship between encounter-rate and prevalence for *E. ewingii* was mainly due to differences in prevalence between sites, whereas the positive association for *Anaplasma phagocytophilum* was sensitive to the extent of pathogen testing coverage. Molecular co-detection of at least two of the selected pathogens was detected in 0.0096% of *A. americanum* and 3.48% of *I. scapularis* nymphs. Systematic non-testing of single-nymph visits and a geographic bias in support preclude inferences outside of those tested ticks and sampled NEON sites. Our study support surveillance reporting intensity of encounters, detection of encounters, prevalence of pathogens in encounters, and coverage of testing separately from an infected-nymph encounter index, as an indicator of absolute density or human disease risk.

Introduction

Tick borne diseases are becoming a growing public health problem in the U.S. The number of reported tick-borne bacterial and protozoan diseases has more than doubled since 2004 and ticks were responsible for the majority of reported vector-borne disease cases since 2004 (Rosenberg et al. 2018). The blacklegged tick, *Ixodes scapularis*, has increased its distribution throughout the eastern United States and is the main vector of several important pathogens of humans (Eisen and Eisen 2018), while the lone star tick, *Amblyomma americanum*, has also expanded beyond much of its historically recognized distribution (Springer et al. 2016; Sonenshine 2018). These changes make surveillance systems that can quantify both the presence of medically important ticks and how their abundance, seasonal activity and pathogen carriage change with time and environment more important (Eisen and Paddock 2021). Several processes take place on different temporal and spatial scales that affect the dynamics of ticks (Randolph 2004; Kache et al. 2023). Ticks are arthropods that are multi-host, ectothermic, and whose development, survival, and host-seeking behaviors are affected by temperature and moisture, but the magnitude and direction of these effects vary among species, life stages, regions and time (Ogden et al. 2021). Climate warming has been suggested to play a role in the geographic distribution and/or abundance of *I. scapularis* in northern parts of the eastern United States; however, climate is not the only factor that accounts for geographic variation (McClure and Diuk-Wasser 2019; Brunner et al. 2023; Eisen and Eisen 2024). Host-seeking ticks are also only available for collection and exposure at specific times of the year, as determined by seasonal phenology (Burtis et al. 2023). During the single sampling visit, the probability of detection and numbers of ticks collected when found can be correlated differently with the environmental factors (Fletcher et al. 2005; Martin et al. 2005). Using a model that

separates tick occurrence/detection from abundance by tick presence allows for the examination of whether environmental conditions are related to occurrence/detection differently than to abundance given the detection of ticks, which would not be possible if these two processes were combined in a single model of zero-heavy counts (Sharma et al. 2024).

Acarological exposure indices are an integration of incidence of tick encounters and of prevalence of infection, but are not tied to human infection risk themselves (Johnson et al. 2018). Risk of human exposure is summarized for *I. scapularis*, often by combining nymphal abundance with pathogen prevalence to calculate density of infected nymphs, and the number of infected, host-seeking nymphs is associated with geographic variation in Lyme disease risk (Pepin et al. 2012; Foster et al. 2023a). *I. scapularis* can carry several bacterial, protozoan and viral pathogens, and ticks are often found to carry more than one pathogen, particularly mixtures of *Borrelia burgdorferi* and *Anaplasma phagocytophilum* and *Babesia microti* (Pepin et al. 2012; Hahn et al. 2018; Johnson et al. 2018; Stewart and Bloom 2020a). *A. americanum* is also an important vector of zoonotic agents especially *Ehrlichia chaffeensis* and *Ehrlichia ewingii* and is often monitored for the presence of *Borrelia lonestari*, a spirochete with documented but infrequently reported human infection, including a molecularly confirmed relapsing-fever case (Childs and Paddock 2003; Maza et al. 2026). The abundance of vectors and prevalence of pathogens does not have to be directly correlated; persistent differences in habitat, hosts and climate can lead to persistent differences in tick abundance and pathogen prevalence, while changes from year to year in abundance within a site need not be tightly coupled to one another (Carbone et al. 2025).

A unique opportunity arises for the study of these processes through standardized, repeated sampling over broad environmental gradients with the National Ecological Observatory Network. NEON uses drag and flag sampling methods to collect host-seeking ticks at terrestrial sites throughout the U.S. and sends a portion of the nymphs to the laboratory for multiple bacterial and protozoan pathogen testing (Paull et al. 2022). These data support broad-scale comparisons of vector and pathogen environmental distributions (Alkishe et al. 2024). A recent NEON analysis focused on spatiotemporal synchrony of *A. americanum* nymph abundance, pathogen prevalence, and lagged climatic conditions (Maza et al. 2026). An opportunity for complementing this is to combine the repeated ecological sampling with short-term weather, hierarchical site-plot-event structure, pathogen-assay quality control, and exact linkage between tested ticks and ecological visits, as well as individual-tick multi-pathogen results. This type of integration can answer questions related to whether environmental impacts primarily affect tick presence or abundance, if pathogen prevalence changes in response to increasing or decreasing tick encounter rates, and if apparent pathogen associations are independent of broad geographic structure.

In this study, we explored 2019–2024 NEON data on ticks and pathogens to answer four related questions. First, we quantified associations between occurrence/detection and abundance of adult and nymphal *A. americanum*, adult *D. variabilis*, and nymphal *I. scapularis* and short-term, interannual, and seasonal weather patterns. Second, we characterized unexplained hierarchical and residual spatial structure in the final ecological models. Third, we examined temporal variation in prevalence of the primary pathogens, reconciled pathogen tested ticks to ecological sampling visits, created a descriptive infected nymph encounter index, and determined if site-year nymph encounter rates were correlated with pathogen prevalence for primary pathogens. Supported associations were then split into within-site and between-site associations and

sensitivity to individual influential sites was assessed. As a secondary analysis, pathogen co-detection was quantified based on results from pathogen assays. The ecological weather/seasonality tests and primary pathogen and integrated encounter-prevalence models represented the inferential core and were supplemented with spatial diagnostics, influential-site analyses and co-detection analyses as diagnostic checks, robustness analyses, and explicitly secondary descriptive analyses rather than additional confirmatory tests. Inference was limited to the sample of NEON sites and sampling framework and was not meant to be construed as representing national pathogen prevalence or human disease risk.

Materials and Methods

NEON tick data and focal groups

Tick sampling records were gathered from the National Ecological Observatory Network (NEON) Ticks sampled using drag cloths product (DP1.10093.001); pathogen results were gathered from the Tick pathogen status (DP1.10092.001) product, as per the current NEON tick-product user guide (Paull 2026). The first ecological and integrated analyses were confined to the period 2019–2024, since tick ecology, pathogen prevalence and precise linkage to the visit-level ecology were performed using the finalized tick ecology visit matrix and were limited to that period of time; earlier pathogen records were stored for only descriptive summary of visit-level coverage for assays. The final model-ready visit matrix had a total of 7,667 physical sampling visits across 286 plots at 46 NEON sites. The sampling area varied between 80 and 180 m^2 of eligible visits. The analysis thus does not represent a probability sample of all U.S. landscapes and repeated standardized sampling within these NEON sites was not treated as random sampling with replacement. The numbers of model-ready physical visits in 2019 were (n = 1,600, followed by 2020 (n = 624), 2021(n = 1,373), 2022 (n = 1,259), 2023 (n = 1,281), and 2024 (n = 1,530). The targeted species and life-stages for analyses involved four species/life-stage combinations that had adequate replicated detections for hierarchical modeling: adult *A. americanum*, nymphal *A. americanum*, adult *D. variabilis*, and nymphal *I. scapularis*. Each valid physical visit was recorded independently by each focal group and a visit with no focal tick detected counted as zero. The binary response is referred to as occurrence/detection because the presence of a species in a field is determined by both ecological occurrence and sampling detection.

Sampling effort, seasonality, and weather covariates

The natural log of sampled area, or sampling effort, was used as an offset in both the tick models. This standardization assumes that the numbers of encounters were proportional to sampled area within the sampled structure; however, the same is not assumed for drag and combined drag and flag observations in which sampling method was also included as a fixed effect. Seasonal variation was accounted for by the first and second Fourier harmonics of day of year (F1, F2, the sine and cosine terms for annual and semiannual cycles, respectively). For all focal responses, the same parsimonious cyclic basis was used to allow direct comparison of the response without choosing the smoothness of the response or adding seasonal complexity a posteriori. A 1-km gridded daily weather product for North America, called Daymet Version 4 R1, was used to link the daily weather to the sampling locations (Thornton et al. 2021, 2022). Standardized deviations in 7-day mean temperature, 7-day vapor-pressure deficit (VPD), and log-transformed 30-day precipitation were used in

the weather models. The climate variables were moderately dependent (maximum absolute Spearman rho = 0.695; maximum absolute Pearson r = 0.588) and were thus included together as a prespecified short-term weather block. Daymet does not measure conditions in the litter layer or near the ground level where ticks reside, so weather coefficients were viewed as correlations with large-scale short-term environmental factors, rather than direct influences on the microclimate of ticks.

Two-part hierarchical modeling of tick occurrence/detection and abundance conditional on detection

There were many zeros in the tick count data and nonzero counts were right-skewed. The two model components were fitted separately for each focal group: (i) occurrence/detection and (ii) abundance conditional on detection, hereafter termed positive abundance. Positive abundance denotes the observed count of focal ticks on visits with at least one detected focal tick (count ≥ 1); it does not represent a population-wide measure of latent abundance. This hurdle formulation was selected because the number collected after detection is not always as relevant to the ecological question as is the number detected during a visit and these can be quite different. Models were fitted in glmmTMB (Brooks et al. 2017). The binary component denotes an observed encounter/detection on a standardized visit. Non-detection on that visit is indicated by a zero count and cannot be an ecologic absence. In the occurrence/detection component, a binomial generalized linear mixed model (GLMM) with complementary log-log link function was used to model presence or absence during an eligible visit. Four seasonal Fourier terms, sampling method, year and site were all fixed effects included as baseline models, the log sampled area offset was also included and random intercepts for plot and sampling event were added. The 3 short-term standardized weather covariates were added to the corresponding weather model. Positive-abundance models included all visits with at least one focal tick (single-tick visits), and visits with no ticks were not included in these models. The distribution of counts was assumed to be zero-truncated negative binomial type 2 and the log link function applied in the modeling of positive counts. The seasonal Fourier terms, sampling method, year, the log of sampled area offset, and random intercepts for site and plot were included in the baseline models. The three short-term weather covariates were added to weather models. The reference categories were dragging sampling and 2019. Likelihood-ratio tests (LRTs) were used most often to evaluate weather effects by comparing the full three-variable weather model to the baseline model. Joint removal of all four Fourier terms was used to assess positive-count seasonality. Each family of prespecified models was applied to the four focal groups using the BH correction (Benjamini and Hochberg 1995). Only individual weather coefficients were interpreted where the model level weather block for the corresponding coefficient was still supported after correction. The 20 positive-abundance year contrasts were grouped into a BH-adjusted family, while the eight sampling-method contrasts were grouped into a BH-adjusted family.

Model diagnostics, prediction, and hierarchical heterogeneity

Model convergence, Hessian status, dispersion, and simulation-based residual diagnostics were evaluated for all final models using DHARMa. Diagnostics for zero-truncated count models were adapted to the truncated support, using a count-of-ones check rather than a conventional zero-inflation test. Occurrence models were evaluated for global uniformity, dispersion, outlier, and residual-versus-predicted quantile diagnostics, and

alternative optimizers were used where numerical sensitivity required. Baseline positive-abundance models were used to generate seasonal predictions with random effects set to zero, year fixed in 2019, and sampled area fixed at the model-specific median. Periods > 90% or 75% of the predicted maximum were interpreted as broad peak windows rather than exact peak dates. Marginal occurrence probabilities for *A. americanum* were calculated across standardized temperature deviations while holding vapor pressure deficit (VPD) and precipitation at their means and were taken on the probability scale. Random-intercept variances were summarized only as within-model measures of unexplained heterogeneity; variance shares were not interpreted as intraclass correlation coefficients or compared across models with different distributions or link functions. *In* Fig. 2, the pointwise 95% Wald intervals were computed on the log-link scale and then transformed back to the 0-truncated NB2 distribution using the estimated dispersion parameter. To ensure the visualization of the ribbon, only those calendar months that had at least 10 positive visits for the focal group pooled across 2019–2024 are included for the confidence ribbons, and the rest of the model curves are represented with faint dashed lines.

The sensitivity of to within-site dependence and support that was unevenly distributed was assessed with 500 whole-site cluster bootstrap resamples per species–stage group. All positive count observations at each sampled site were stored in a single container, and their time and plot were indicated, with sampled sites repeated in the container assigned a different bootstrap site/plot label. For every refit, the year coefficient ratio corresponding to the 2019 year was extracted from the baseline model (hierarchical truncated-NB2), and the unadjusted percentile 95% intervals were numerically calculated from the replicates. Complementary influence screen: leave-one-site-out fits. The analysis of nymphal *A. americanum* had 500/500 valid replicates, the analysis of adult *D. variabilis* had 494/500 valid replicates and the analysis of nymphal *I. scapularis* had 493/500 valid replicates. All flag-method positive encounters of adult *A. americanum* were limited to a single location (UKFS) and resulted in many site resampling failures of rank/design. The key 550-record model was used as the primary model, and a separate 545-record drag only/restricted method sensitivity analysis was performed (500/500 valid resamples). The sensitivity estimates provided in these cluster-bootstrap intervals were not considered multiplicity adjusted inferential tests. Grouped sampling via the site bootstrap was evaluated for the impact on year contrasts but does not explicitly estimate a temporal correlation function; temporal association was identified using exact date within plot residual screens in both *A. americanum* groups. No observed numerical difference in any of the 16 revised seasonal and weather count-model fits in terms of coefficients, fixed-effect standard errors, log-likelihoods, or predicted means under R 4.6.0, glmmTMB 1.1.14 and matched TMB 1.9.21.

Residual Spatial Dependence

Additionally, residual spatial dependence was not viewed as a new predictor selection exercise, but rather as a model diagnostic. The spatially aggregated DHARMa residuals were assessed using Moran's I (Moran 1950), with exact permutation checks for focal models showing residual structure and BH correction across the tested models. Targeted distance-band diagnostics were then made to see if any specific spatial scale was predominant. Exponential sensitivity models for the spatial-covariance structure of the residuals were fitted for nymphal *A. americanum* and nymphal *I. scapularis* occurrence models, where residual spatial autocorrelation was found. The spatial model for *A. americanum* nymphs was not retained for inference, but it was explicitly

identified as a limitation of the main nonspatial model, because the fitted model had a non-positive-definite Hessian. Spatial model of the nymphal *I. scapularis* was estimable and removed the residual Moran signal but did not increase likelihood and only added four units to AIC. Primary nonspatial hierarchical models were used, and the coefficients from the responses that showed residual spatial structure were read as associations rather than spatially independent or causal effects. Predictor and covariance searches were not expanded after this prespecified stage to obtain spatial sensitivity analyses.

Pathogen assay processing and quality control

The NEON tick pathogen status product (DP1.10092.001) was used to acquire pathogen records. The product is defined at the individual tested tick and pathogen target level and a subset of positive identified nymphs are tested for bacterial and protozoan pathogens (Paull 2026). Multiple pathogen target records may exist for each tick, so the biological testing unit was the testingID (not the number of assay rows). Pathogen-specific denominators included only explicit Positive or Negative results and blank or unreported results were excluded. There are no conflicting duplicated records (testingID and pathogen). Of the 175,549 tests after DNA-quality and eligibility filtering, 128,054 tests had documented batch-QA pass information. Three historical batches (2016, 2017, and 2019) have no retrievable QA records and were deemed QA unavailable instead of failed. The descriptive summary of whole-period pathogen coverage was provided for 2014–2024, and the modelling of prevalence was only conducted over the period 2019–2024 for consistency in time. The prevalence estimates provided were based on pathogen models and only included tested ticks; they are not counts of all ticks collected or national prevalence.

Selection and modeling of pathogen effects

Eight species; lifestage–pathogen combinations had sufficient positives and replication for structural assessment: *B. lonestari*, *E. chaffeensis*, and *E. ewingii* in nymphal *A. americanum*; and *B. burgdorferi* sensu lato, *A. phagocytophilum*, *B. microti*, *B. miyamotoi*, and *E. muris*-like (*E. muris eauclairensis*) in nymphal *I. scapularis*. The first 5 pathogens were selected as the primary panel for inferential analysis in 2019–2024 after evaluating distribution of positives across sites, plots, events, years and seasons. *B. microti* was limited to two sites and *E. muris*-like and *B. miyamotoi* had marginal and sporadic temporal or event-level distributions and were therefore only kept for descriptive or exploratory analysis. Binomial logistic mixed models were used for pathogen prevalence of primary *I. scapularis*. The *B. burgdorferi* s.l. model had site and plot random intercepts with year and season as fixed effects, while the *A. phagocytophilum* model had a single site random intercept and the fixed effect of continuous year (due to absence of positives in one year). Overdispersion was found with the initial individual-tick Bernoulli models, and the final inference for the three pathogens of *A. americanum* was done using event-aggregated beta-binomial models. The simpler valid random-effects model structure within 2 AIC units of the best-supported model was used: plot random intercept for *E. chaffeensis* and *E. ewingii*, no additional random intercept for *B. lonestari*. Omnibus LRTs (Likelihood Ratio Test) and BH adjustment of year and season were performed. Estimated marginal means and all pairwise year contrasts for supported year effect *E. ewingii* were obtained using the emmeans package (Lenth 2023) primary pairwise contrasts done with Tukey adjustment.

Pathogen-testing linkage and integrated infected-nymph encounter index

The primary ecological sampling matrix was matched to pathogen-tested nymphs by exact site, plot and collection date prior to integration with tick counts. Tests did not have to be rearranged to adjacent or less detailed site-year-season cells during pathogen-only visits, and exact matching ensured that tested numbers of nymphs were not higher than during the matching ecological visits. The number of nymphs collected from each ecological visit (including visits with no nymphs collected) was divided by the area sampled, in meters squared, to calculate the encounter rate. The prevalence of pathogens was estimated based on exact-matched tested nymphs and the infected-nymph encounter index was estimated (encounter rate × pathogen prevalence). This index is not a true measure of field density, but of standardized encounter intensity. Its 95% intervals were for pathogen-prevalence uncertainty, keeping the encounter rate constant. The overall, year-by-year and site-year-by-site-year testing coverage was summarized and estimates for integrated testing were restricted to site-years in which pathogen testing had been performed. A nymph sensitivity analysis was conducted using high-support site-years, those for which ≥ 20 nymphs were tested and ≥ 50% testing coverage was obtained. Pathogen testing was not thought to be a simple random sample of all nymphs collected. The index assumes that the prevalence of tested-nymphs is informative of collected-nymphs' prevalence, which cannot be proven by high support restrictions or model sensitivity analyses.

Additionally, pathogen tested nymphs were compared to counts of these nymphs as seen in the field using site, plot and date of collection in exact-match reconciliation. In the nymph positive visits, assay availability was compared to the number of nymphs collected to determine if it was related to the number of nymphs collected per visit. Pathogen-only tests that were not associated with an eligible ecological visit were included in descriptive assays inventories only and were not included in encounter–prevalence model denominators. The observed counts of tests were interpreted as a characteristic of the analytical record, rather than as evidence of an implicit universal rule for selection of laboratories at NEON.

Association between nymph encounter rate and pathogen prevalence

The infected nymph encounter index was used to test if site-years with higher encounter rates also had a higher pathogen prevalence, but encounter rate is a multiplicative component of the encounter index. Instead, nymphs were directly modeled as a binomial response, with the log1p-transformed site-year nymph encounter rate as the predictor of interest. Encounter-rate standardization, at the vector-species level, was conducted. For the three pathogen outcomes of *A. americanum*, beta-binomial mixed models were used, while binomial logistic mixed models were used for the two pathogen outcomes of *I. scapularis*. A site random intercept was added to all models to account for repeated site-years. The pathogen temporal analyses were performed with a categorical factor to represent *B. lonestari*, *E. chaffeensis*, *E. ewingii*, and *B. burgdorferi* sensu lato, and a centered continuous year term to represent *A. phagocytophilum*. The encounter-rate effect was tested by likelihood-ratio test (LRT) for the full model against the reduced model without the encounter-rate term, for the five prespecified pathogen outcomes, with BH correction (Benjamini and Hochberg 1995). The primary models contained all site-years eligible for pathogen tests (*A. americanum* = 55; and *I. scapularis* n = 48), and a high-support sensitivity analysis was limited to site-years in which at least 20 nymphs were tested and at least 50%

of the nymphs were tested (37 and 27 site-years, respectively). Testing fraction defined the high support set and was also included as a standardized covariate in an exploratory sensitivity analysis; testing fraction and encounter rate were both derived from the same catch process and therefore were not considered to be an independently validated covariate to correct for selection bias. Convergence, Hessian status and DHARMa simulation-based residual diagnostics were used to assess the model adequacy (Hartig 2016).

An exploratory binomial mixed-model sensitivity analysis was retested to the original site-year data for two key outcomes of *I. scapularis*. The original encounter predictor scaling, outcome-specific year effect and site random intercept were kept. Each of the following models was compared: (1) with no standardized testing fraction; (2) with high-support subsets; (3) with decompositions of the rate of encounters and standardized testing fraction to the site means and deviations from these means, respectively. Two types of tested residual checks (Akaike information criterion, convergence, Hessian status, and simulation-based DHARMa) were reviewed, as well as same-data likelihood-ratio tests for comparing nested specifications. The post hoc sensitivity analyses were not considered as independent confirmatory analyses, nor as estimates of a selection-corrected population prevalence.

Within-site, between-site, and leave-one-site-out analysis

Log-transformed nymph encounter rate was split into a between-site component (site mean over the years sampled) and within-site component (annual deviation from site mean). The components were standardized individually. All decomposition models contained the within-site and between-site encounter terms, the outcome specific year of term, and a site random intercept. LRTs were conducted for each component between the full model and the corresponding model without the component. BH adjustment was used separately for the five within-site tests, the five between-site tests, as well as a conservative sensitivity BH correction across all 10 component tests. For outcomes that were supported by the primary total encounter-rate analysis, leave-one-site-out sensitivity models were fitted by leaving each site out, one at a time, and refitting the total encounter-rate model. The largest number of pathogen positives was identified separately and explicitly examined after excluding it from the site. Robustness was assessed not based on all reduced data refits also having nominal significance, but by the numerical validity, the direction of the effect, the magnitude of the effect and uncertainty.

Complementary, and related to the number of nymphs collected at each visit, a pathogen positivity for the nymphs tested during each visit to the logarithm of the number of nymphs collected. The total number of tested nymphs and the number of positive tested nymphs were fixed for each site-year, but the infection statuses were re-distributed under a conditional multivariate hypergeometric null model with a 2-sided Monte Carlo P value for each visit. An exploratory test for the first 2-pathogens employed 4999 simulations, while focused tests of B. burgdorferi sensu lato influence employed 9999 simulations. Each of the following was omitted from the sensitivity list: each site, TREE in 2019, visits with 20 or more nymphs, and excluding TREE and large catches. It is important to note that the exchangeability assumption is only for tested nymphs within a site-year and not visit-level clustering nor infection status among untested nymphs is addressed by the permutation procedure.

Individual tick pathogen co-detection analysis

Pathogen co-detection was evaluated as a secondary analysis at the individual tested-tick level with testingID. Only 2019–2024 and certain pathogen outcomes were considered, with explicit binary results. The co-detection panel included *B. lonestari*, *E. chaffeensis*, and *E. ewingii* for nymphal *A. americanum*; and *B. burgdorferi* sensu lato, *A. phagocytophilum*, *B. microti*, *B. miyamotoi*, and *E. muris*-like for nymphal *I. scapularis*. A broad *Borrelia* sp. screen was not included as it was an umbrella assay and *B. mayonii* was not included in inferential pairwise analysis due to the overlapping interpretation with the *B. burgdorferi* sensu lato assay. The 2 x 2 table includes only ticks that were tested for both pathogens. Pairwise association was measured by Fisher exact odds ratios and exact P-values and double positive counts compared to the number expected under independence. The Benjamini-Hochberg procedure was used to correct for p-values within and between vector species. Site-stratified Mantel-Haenszel analyses were conducted as a robustness check as only sites in which both pathogen outcomes varied contributed to the stratified association. Molecular co-detection was not considered a mechanistic interaction between the pathogens. Site-stratified analyses dealt with spatial confounding at a broad level but were unable to control for residual spatial clustering within sampling events or shared hosts. Fisher and site-stratified effects were considered directionally concordant when the signs were the same and effects were significant following BH within vectors. In addition to summarizing complete-panel ticks by numbers of selected pathogens detected (0, 1, 2, ≥ 3), they were summarized by combinations of pathogens that were positive. These findings were termed co-detection or co-positivity and not confirmed biological coinfection.

Inferential hierarchy, multiplicity, and scope of inference

Analyses were grouped into biologically defined families of inferential tests instead of being considered as a single family of significance tests. Prespecified primary ecological families comprised four occurrence weather-block tests, four positive-abundance weather-block tests, four positive-abundance seasonality tests, 20 positive-abundance year contrasts, and eight sampling-method contrasts. In the selected pathogen panel, the primary pathogen temporal tests were evaluated. The results of the integrated encounter-prevalence effects constituted a family of five outcomes; the within-site and between-site decomposition tests were adjusted as separate families of five tests with an added all-10 BH correction, reported as a conservative sensitivity. Secondary individual-tick co-detection analyses used BH adjustments within vector species and across the full set of tested pathogen pairs. The diagnostic checks, spatial sensitivity fits, high-support restrictions and leave-one-site-out refits were not considered as separate discovery claims; they were used to evaluate the model adequacy or model robustness. The unadjusted coefficients were only interpreted within the context of the specific supported model block or a prespecified contrast family throughout the study. The infected-nymph encounter index is a descriptive index, rather than a measure of absolute density of infected-nymphs or risk of human disease.

Results

Tick detections and abundance across focal species and life stages

In total, there were 2,995 positive sampling records across the four focal response matrices, and 27,673 focal group zeros for the 7,667 physical visits. Adult *A. americanum* was detected on 550 visits and yielded 2,445

ticks; nymphal *A. americanum* was detected on 1,154 visits and yielded 12,633 ticks; adult *D. variabilis* was detected on 573 visits and yielded 1,153 ticks; and nymphal *I. scapularis* was detected on 718 visits and yielded 2,908 ticks (Table 1).

Table 1
Focal tick groups and analytical support in the final ecological models.

Focal group	Occurrence/detection N	Positive-abundance N	Ticks in positive records
A. americanum adult	3,456	550	2,445
A. americanum nymph	3,456	1,154	12,633
D. variabilis adult	4,889	573	1,153
I. scapularis nymph	3,525	718	2,908

Footnotes: Prior to focal-specific support restrictions, there were 7,667 physical visits for each focal stratum in the model ready visit matrix. Only visits where at least one focal tick was detected are included in positive abundance models. For each, Sites / plots were 46 / 286 and period was 2019–2024.

Short-term weather was associated with A. americanum detection but not positive abundance

The three-variable short term weather block enhanced the occurrence/detection model for both *A. americanum* life stages (Table 2). For adults, the weather block gave LR = 10.86 with 3 df (*P = 0.0125; BH-adjusted P = 0.0251*). For nymphs, LR = 12.12 (*P = 0.0070*; *BH-adjusted P = 0.0251*). The occurrence/detection of adult *D. variabilis* (*BH-adjusted P = 0.6140*) and nymphal *I. scapularis* (*BH-adjusted P = 0.2256*) were not supported by weather models. In the supported *A. americanum* models, the occurrence/detection of both adults (beta = 0.181, SE = 0.083, *P = 0.0294*) and nymphs (beta = 0.206, SE = 0.074, *P = 0.0051*) was positively associated with standardized 7-day mean-temperature deviation. These blocks did not have comparable independent evidence from VPD or 30-day precipitation. Adults and nymphs of *A. americanum* each showed higher occurrence/detection (at + 1 SD than at -1 SD) on the probability scale (Fig. 1). The adult *A. americanum* occurrence model did not show the residual spatial-autocorrelation signal detected in the nymphal model. Since there was still substantial spatial autocorrelation in the final occurrence model for *A. americanum* nymphs and the spatially-covariance sensitivity fit was not estimable, the temperature nymphal outcome was taken as an association in the retained hierarchical specification not as causal effect or a spatially independent effect. However, unlike the occurrence/detection block, no positive-abundance block was supported following multiple-testing correction. Model-level tests yielded for adult *A. americanum* (P = 0.0958), nymphal *A. americanum* (*P = 0.0702*), adult *D. variabilis* (*P = 0.3927)*, and nymphal *I. scapularis* (*P = 0.0458*); the corresponding BH-adjusted P-values were 0.1277, 0.1277, 0.3927, and 0.1277, respectively (Table 2). *I. scapularis* therefore was a nominal outcome.

Table 2
Omnibus weather and positive-abundance seasonality tests for the four focal tick groups.

Focal group	Occurrence weather LR (df)	P	BH P	Positive-abundance weather LR (df)	P / BH P	Positive-abundance seasonality
A. americanum adult	10.86 (3)	0.0125	0.0251	6.35 (3)	0.0958 / 0.1277	48.52 (4); BH 9.82e-10
A. americanum nymph	12.12 (3)	0.0070	0.0251	7.06 (3)	0.0702 / 0.1277	93.31 (4); BH 5.22e-19
D. variabilis adult	1.80 (3)	0.6140	0.6140	2.99 (3)	0.3927 / 0.3927	31.78 (4); BH 2.12e-06
I. scapularis nymph	5.04 (3)	0.1692	0.2256	8.01 (3)	0.0458 / 0.1277	113.23 (4); BH 5.95e-23

Footnotes: Positive-abundance weather likelihood-ratio tests were independently recreated for four sets of group-level observations (n = 550, 1,154, 573, and 718) fitted to the same models. Four weather-block BH-adjusted P-values were 0.1277, 0.1277, 0.3927, and 0.1277. The weather results for the occurrence models are identical to the results in the original weather model. Stage 14B did not have its own weather result for the occurrence models.

Seasonal variation in tick abundance at positive sampling visits

There was significant seasonal structure for all four focal groups in positive abundance (Table 2; Fig. 2). Joint tests of the four Fourier terms yielded LR = 48.52 for adult *A. americanum* (BH P = 9.82×10^{-10}), LR = 93.31 for nymphal *A. americanum* (BH P = 5.22×10^{-19}), LR = 31.78 for adult *D. variabilis* (*BH P = 2.12×10^{-6}*), and LR = 113.23 for nymphal *I. scapularis* (*BH P = 5.95×10^{-23}*). Focal groups had varying magnitudes of seasonality. The peak-to-trough ratio for adult *A. americanum* was 1.48 and for nymphal *A. americanum* was 1.92, and both had a window of at least 90% of the modeled maximum, respectively, from about April 28-June 27 and from May 18 - July 5. For adults of *D. variabilis*, the revised positive-count model showed modest seasonal variation (peak-to-trough ratio 1.23), with a window at or above 90% of its annual maximum from April 23 to August 3. The 75%-of-maximum criterion was not biologically informative because the conditional mean of a zero-truncated count model cannot fall below one tick. The highest concentration of nymphal *I. scapularis* (ratio = 2.76) was from the 13th of May to the 14th of June (at least 90%).

Interannual variation in positive abundance and site-bootstrap sensitivity

The primary hierarchical zero-truncated NB2 analysis yielded 11 of 20 BH-adjusted Wald-significant year coefficients relative to 2019 (Table 3; *Supplementary Table S3*). These exponentiated coefficients describe ratios of the underlying NB2 mean parameter, not directly the ratios of expected counts conditional on detection. Site-resampled sensitivity analyses indicated substantially wider uncertainty for several contrasts. In the primary-model bootstrap analyses, unadjusted 95% intervals excluded unity for adult *D. variabilis* in 2021–2024 and nymphal *I. scapularis* in 2020, but not for either year contrast in nymphal *A. americanum*. In a restricted 545-record analysis of adult *A. americanum*, excluding five UKFS flag visits, intervals excluded unity

for 2020 and marginally for 2022 (upper bound 0.993). The 550-record primary estimates were retained. These bootstrap intervals were not multiplicity-adjusted and should not be counted as confirmed discoveries. All eight sampling-method contrasts were nonsignificant after BH adjustment.

Table 3
Positive-abundance year contrasts meeting BH-adjusted Wald P < 0.05 in primary hierarchical zero-truncated NB2 models, with site-cluster bootstrap sensitivity (reference 2019).

Focal group	Year	NB2 μ ratio	Wald 95% CI	BH P	Site bootstrap 95% CI	Bootstrap analysis
Adult *A. americanum*	2020	0.522	0.325–0.839	0.01623	0.276–0.701	Restricted 545*
Adult *A. americanum*	2022	0.607	0.425–0.865	0.01428	0.382–0.993	Restricted 545*
Nymphal *A. americanum*	2021	1.519	1.178–1.959	0.00501	0.893–2.590	Primary
Nymphal *A. americanum*	2024	1.411	1.090–1.826	0.01768	0.528–3.377	Primary
Adult *D. variabilis*	2020	2.535	1.187–5.414	0.02959	0.699–4.595	Primary
Adult *D. variabilis*	2021	2.131	1.252–3.627	0.01428	1.068–3.687	Primary
Adult *D. variabilis*	2022	2.219	1.291–3.813	0.01309	1.220–4.598	Primary
Adult *D. variabilis*	2023	3.996	2.422–6.593	1.172e-06	1.689–7.485	Primary
Adult *D. variabilis*	2024	2.757	1.672–4.547	0.0004687	1.454–4.581	Primary
Nymphal *I. scapularis*	2020	0.384	0.254–0.580	5.647e-05	0.230–0.767	Primary
Nymphal *I. scapularis*	2022	0.567	0.418–0.768	0.001256	0.303–1.218	Primary

Footnotes: The underlying NB2 mean parameter μ is represented by ratios of exp(year coefficients) and not the ratios of the expected counts given detection. BH P are adjusting 20 main Wald tests. The bootstrap values are 500 resamples of the whole-site that preserves within-site observations, and are sensitivity estimates, not multiplicity-adjusted tests. Adult A. americanum bootstrap intervals are derived from a restricted-method sensitivity fit that does not include the five UKFS flag visits, and the primary estimates and BH P use all 550 positive visits. A bootstrap interval that crosses 1 show that the Wald significance is sensitive to this analysis. The complete 20-contrast results are given in Supplementary Table S3.

Site and plot-level heterogeneity in tick occurrence and abundance

In occurrence/detection models, the random-intercept variance was highest at the plot level, with 82.3% of the variance for adults and 79.1% for nymphs of *A. americanum*. Plot-level heterogeneity accounted for 55.9% and 57.0% of the retained random-intercept variance for adult *D. variabilis* and nymphal *I. scapularis*, respectively

(*Supplementary Table S1*; Fig. 3). The contributions from sites and plots were almost equal for abundance of adult *A. americanum*, nymphal *A. americanum*, and adult *D. variabilis*. This was very different for nymphal *I. scapularis*, where 76.6% of the retained random-intercept variance was at the site level and 23.4% at the plot level. All retained components had nonzero estimated variance. The raw magnitudes of the variance and their contribution to the model are presented in Fig. 3. The percentages are relative allocations of random-intercept heterogeneity within each model and are not intra-class correlation coefficients (ICCs).

Residual spatial autocorrelation in nymphal tick occurrence models

Residual spatial autocorrelation was detected in the nymphal *A. americanum* occurrence model using exact permutation tests (*P = 0.0001; BH P = 0.0002*) and in the nymphal *I. scapularis* occurrence model (*P = 0.0307; BH P = 0.0307*), although the latter signal was weaker. Residual maps and distance-band correlograms are shown in *Supplementary Fig. S1*. No specific distance band remained significant after BH correction, so the residual signal was not assigned to a particular spatial scale. None of the four positive-abundance models showed strong residual spatial autocorrelation. For nymphal *A. americanum*, the exponential spatial sensitivity model converged but had a non-positive-definite Hessian and was not suitable for inference. For nymphal *I. scapularis*, the spatial model was estimable and removed the residual Moran signal but did not improve likelihood and increased AIC by four units (2107.40 versus 2103.40). Spatial covariance was therefore not added to the primary models. Smaller but significant combined residual-versus-predicted quantile deviations occurred in both baseline and weather nymphal *I. scapularis* occurrence models and were taken cautiously.

Pathogen testing coverage and prevalence during 2014–2024

Across the 11 calendar years 2014–2024, 18,254 nymphs of *A. americanum* were tested with valid assay outcomes for the main pathogens associated with this tick species. *B. lonestari* was detected in 133 ticks (0.729%), *E. chaffeensis* in 100 (0.548%), and *E. ewingii* in 164 (0.898%; Table 4). One nymph was positive for *A. phagocytophilum* and no *F. tularensis* or *R. rickettsii* were found in the *A. americanum* panel. Among 3,834 tested nymphal *I. scapularis*, *B. burgdorferi* sensu lato was detected in 762 ticks (19.875%), *A. phagocytophilum* in 118 (3.078%), *B. microti* in 109 (2.843%), *B. miyamotoi* in 56 (1.461%), and *E. muris*-like in 25 (0.652%; Table 4). *B. mayonii* was only found seven times and was descriptively retained. The broad *Borrelia* assay was not considered as a separate pathogen group as the positives in the broad and specific *Borrelia* assays were strongly overlapping; all 133 *B. lonestari* positives in *A. americanum* and all 762 *B. burgdorferi* sensu lato positives in *I. scapularis* were broad *Borrelia* assay positive.

Table 4
Pathogen prevalence support and final analytical role for the eight-candidate nymphal tick-pathogen outcomes

Tick	Pathogen	Tested 2014-24	Positive 2014-24	Tested 2019-24	Positive 2019-24	Analytical role
A. americanum nymph	*B. lonestari*	18,254	133 (0.729%)	10,382	67 (0.645%)	Primary; beta-binomial
A. americanum nymph	*E. chaffeensis*	18,254	100 (0.548%)	10,382	62 (0.597%)	Primary; beta-binomial
A. americanum nymph	*E. ewingii*	18,254	164 (0.898%)	10,382	135 (1.300%)	Primary; beta-binomial
I. scapularis nymph	*B. burgdorferi* sensu lato	3,834	762 (19.875%)	2,298	452 (19.669%)	Primary; logistic GLMM
I. scapularis nymph	*A. phagocytophilum*	3,834	118 (3.078%)	2,298	63 (2.742%)	Primary; logistic GLMM
I. scapularis nymph	*B. microti*	3,834	109 (2.843%)	2,298	77 (3.351%)	Descriptive/exploratory
I. scapularis nymph	*B. miyamotoi*	3,834	56 (1.461%)	2,298	29 (1.262%)	Descriptive
I. scapularis nymph	*E. muris*-like	3,834	25 (0.652%)	2,298	21 (0.914%)	Descriptive

Footnotes: Only ticks that have specific binary results for the specified target are included in prevalence denominators. Main temporal inferences were not derived from descriptive/exploratory outcomes due to few or concentrated positive supports.

Pathogen Prevalence during the 2019–2024 ecological study period

Restriction to 2019–2024 yielded 10,382 tested nymphal *A. americanum* from 13 sites and 56 plots (Table 4): 67 *B. lonestari* positives (0.645%), 62 *E. chaffeensis* positives (0.597%), and 135 *E. ewingii* positives (1.300%). A total of 452 *B. burgdorferi* sensu lato (19.669%) and 63 *A. phagocytophilum* (2.742%) were found in 2,298 ticks tested from 10 sites and 43 plots in total for nymphal *I. scapularis* (Table 4). Nonprimary outcomes included 77 *B. microti* (3.351%), 29 *B. miyamotoi* (1.262%), and 21 *E. muris*-like positives (0.914%) (Table 4). No evidence of year and season effects was observed in the final logistic mixed models of the two main *I. scapularis* outcomes following BH. For *B. burgdorferi* sensu lato, the year block gave LR = 8.99 with 5 df (P = 0.1096; BH P = 0.4033) and season gave LR = 2.66 with 2 df (P = 0.2648; BH P = 0.5138). *A. phagocytophilum* likewise showed no continuous temporal trend (LR = 1.37, df = 1, P = 0.2420; BH P = 0.4033) and no seasonal effect (LR = 0.12, df = 2, P = 0.9415; BH P = 0.9415). The diagnostics for DHARMa were clean for both final logistic models.

Ehrlichia ewingii prevalence varied among years

Event-aggregated beta-binomial models eliminated the overdispersion observed in the initial individual-tick Bernoulli models for the three primary *A. americanum* pathogens, while the two final *I. scapularis* logistic models had acceptable residual diagnostics. Final *A. americanum* beta-binomial DHARMa dispersion P-values were 0.418 for *B. lonestari*, 0.224 for *E. chaffeensis*, and 0.106 for *E. ewingii*. No seasonal effect was supported for any of the three pathogens (Table 5). Year was also unsupported for *B. lonestari* (LR = 7.63, df = 5, P = 0.1776; BH P = 0.2663) and *E. chaffeensis* (LR = 6.21, df = 5, P = 0.2859; BH P = 0.2859). *E. ewingii* prevalence varied significantly among years (LR = 17.60, df = 5, P = 0.00349; BH P = 0.0105 within the year-test family; BH P = 0.0210 across all six *A. americanum* year/season tests), and this result was robust to optimizer choice. Adjusted *E. ewingii* prevalence was 0.440% in 2019, 0.377% in 2020, 0.235% in 2021, 0.789% in 2022, 0.929% in 2023, and 0.226% in 2024 (Table 5). Tukey-adjusted comparisons supported higher prevalence in 2023 than in 2021 (2021 versus 2023 OR = 0.251, 95% CI 0.108–0.587, P = 0.0177) and 2024 (OR = 4.146, 95% CI 1.722–9.983, P = 0.0189).

Table 5
Primary pathogen temporal tests and supported Ehrlichia ewingii year contrasts, 2019–2024.

Panel A. Final primary pathogen temporal tests							
Pathogen	**Final model**	**Year LR (df)**	**P**	**Year BH P**	**Season LR (df)**	**P**	**Season BH P**
B. lonestari	Beta-binomial	7.63 (5)	0.1776	0.2663	1.24 (2)	0.5372	0.5372
E. chaffeensis	Beta-binomial	6.21 (5)	0.2859	0.2859	5.93 (2)	0.0517	0.1550
E. ewingii	Beta-binomial	17.60 (5)	0.0035	0.0105	1.62 (2)	0.4457	0.5372
B. burgdorferi sensu lato	Logistic GLMM	8.99 (5)	0.1096	0.4033	2.66 (2)	0.2648	0.5138
A. phagocytophilum	Logistic GLMM	1.37 (1)	0.2420	0.4033	0.12 (2)	0.9415	0.9415
Panel B. Adjusted Ehrlichia ewingii prevalence by year and Tukey-supported pairwise contrasts							
Year	**Adjusted prevalence**	**95% CI**					
2019	0.440%	0.172–1.121%					
2020	0.377%	0.127–1.117%					
2021	0.235%	0.088–0.629%					
2022	0.789%	0.341–1.814%					
2023	0.929%	0.408–2.101%					
2024	0.226%	0.081–0.626%					
Panel C. Primary Tukey-supported pairwise contrasts							
Contrast	**OR**	**95% CI**	**BH P**	**Tukey P**			
2021–2023	0.251	0.108–0.587	0.0113	0.0177			
2023–2024	4.146	1.722–9.983	0.0113	0.0189			

Footnotes: Temporal tests for A. americanum pathogens, and for I. scapularis pathogens tests from final logistic GLMMs. A. phagocytophilum year was continuous. The main post-hoc procedure was Tukey adjustment, and the direction of the contrast was included as OR.

Pathogen-testing linkage and integrated infected-nymph encounter index

Visit-level reconciliation of pathogen tested *A. americanum* nymphs with primary ecological visits resulted in a match of 10,159/10,382 (97.9%) and of pathogen tested *I. scapularis* nymphs with primary ecological visits

resulted in 2,188/2,298 (95.2%). In exact matching, the number of pathogens tested nymphs was not greater than the number collected during each of the corresponding ecological visits. Of the 55 positive *A. americanum* site-years and 48 positive *I. scapularis* site-years ordered for testing, 99.8% and 99.0%, respectively, of all the collected focal nymphs were from these ordered site-years. However, most of the cells with no pathogen testing were low count cells (Table 6).

Table 6
Exact pathogen-testing linkage and site-year support for integrated tick-pathogen analyses.

Vector-pathogen outcome	Exact matched tests	Exact match	Integrated site-years	High-support site-years	Median tested/site-year	Median testing
A. americanum - B. lonestari	10,159 / 10,382	97.9%	55	37	88	79.7%
A. americanum - E. chaffeensis	10,159 / 10,382	97.9%	55	37	88	79.7%
A. americanum - E. ewingii	10,159 / 10,382	97.9%	55	37	88	79.7%
I. scapularis - B. burgdorferi s.l.	2,188 / 2,298	95.2%	48	27	26.5	60.4%
I. scapularis - A. phagocytophilum	2,188 / 2,298	95.2%	48	27	26.5	60.4%

Footnotes: Pathogen-tested nymphs and coverage of at least 50% were present at the primary-support sites-years. Site, plot and collection date were used for exact matching.

Visit-level pathogen-testing allocation and matching discrepancies

The 2,298 *I. scapularis* nymphs tested in the 2019–2024 assay inventory included 2,188 tests exactly linked to eligible ecological sampling visits (95.2%) and 110 tests were distributed among 13 pathogen-only visit records. Among these tests with no match, 58 tests were picked on the same date and same site, and 52 did not have an available site–date record. There was a difference of seven site-years, with 79 unmatched records in 2023 at Harvard Forest & Quabbin Watershed (HARV), Massachusetts (HARV). The older seasonal inventory at HARV in summer 2023 contained 210 tests, while the restricted ecological dataset contained 151 nymphs, which represents 139.1% of the former data not used as an ecological testing-coverage denominator (*Supplementary Table S4*).

With the exact-visit level, 716/718 (99.72%) of the *I. scapularis* visits with nymphs were matched with exactly one less tested nymph than collected nymphs; two of the visits with nymphs were matched with two fewer nymphs than collected nymphs. A similar disparity of one nymph was seen in 1,133 of 1,154 (98.18%) visits by *A. americanum* positive nymphs. Among all 718 *I. scapularis* nymph-positive visits, 293 had no matched pathogen tests and included 292 visits by single nymphs. The 688 positive visits in the 48 site-years of *I. scapularis* used in the integrated models yielded 2,878 collected nymphs, with only 2,188 of those nymphs being tested, and none of the 262 single nymph visits in these site-years were tested. The number tested was recomposed exactly as 2,878 − 688 positive visits - two additional unassayed nymphs. The mean collection

size per positive visit is structurally coupled to testing coverage in the form of a near deterministic relationship (Spearman's rho = 0.99967) between the two (*Supplementary Table S4*). The observed nymph encounter rate and exact-matched pathogen prevalence were used to calculate an infected-nymph encounter index (Fig. 4). The highest annual estimates of infected-nymph encounters per 100 m^2 for pathogen testing were for *I. scapularis-B. burgdorferi* sensu lato (0.053–0.265). For *A. americanum-E. ewingii*, the annual index increased from 0.013 in 2021 to 0.062 in 2022 and 0.097 in 2023 before declining to 0.020 in 2024 (Fig. 4). These values were not considered to be absolute density of infected nymphs but rather as descriptive exposure indices. They only carry uncertainty of pathogen prevalence and do not constitute the full uncertainty of the product, as interpretation also relies on the assumption that the pathogen prevalence in the subset of the product being tested is representative of the whole within each site-year analyzed.

Nymph encounter rate was associated with prevalence for two pathogen outcomes

Across matched site-years, higher log-transformed nymph encounter rate was associated with higher prevalence of *E. ewingii* in *A. americanum* nymphs (OR = 3.30 per 1-SD increase, 95% CI 2.03–5.37; LR = 13.12, P = 0.000292; BH P = 0.00146) and *A. phagocytophilum* in *I. scapularis* nymphs (OR = 1.47, 95% CI 1.13–1.90; LR = 6.88, P = 0.00873; BH P = 0.0218) (*Supplementary Table S2*; Fig. 5A). For the other three pathogen outcomes, there was no post adjustment support. Positive associations were retained for *E. ewingii* (OR = 3.46 (BH P = 0.00252)) and *A. phagocytophilum* (OR = 1.45 (BH P = 0.0403)) when a high-support sensitivity was used, that included only site-years that had at least 20 nymphs tested and had at least 50% tested. Supported primary models had positive definite Hessians with no significant uniformity, dispersion or outlier departures for DHARMa. These total site-year associations were thus retained for the interpretation of within-site/between-site decomposition instead of a direct interpretation as temporal coupling.

Supported encounter-prevalence associations were primarily between sites

The within-site and between-site components of encounter rate were separated and for each site the strongest associations were with spatial variation between sites, rather than year-to-year variation within the site (*Supplementary Table S2*; Fig. 5B). The between-site component was strongly positive for *E. ewingii* (OR = 3.04, 95% CI 1.94–4.77; *LRT P = 0.00240*; BH *P = 0.0120*) and was still supported after conservative correction for all ten within- and between-site component tests (OR = 3.04, 95% CI 1.94–4.77; adjusted *P = 0.0240*). Within-site effect was marginally positive (OR = 1.64; *P = 0.0350*) but didn't pass the BH correction (*BH P = 0.175*). For *A. phagocytophilum*, the between-site effect also was positive (OR = 1.48, 95% CI 1.11–1.97; P = 0.0162; *BH P = 0.0405*), whereas the within-site component was unsupported (OR = 1.15; *BH P = 0.391*). The P value for the between-site *A. phagocytophilum* result did not become significant with correction (adjusted *P = 0.0811*) across all 10 component tests. The unadjusted Wald interval cannot be interpreted as a multiplicity adjusted significance test, as a positive between-site estimate for *B. burgdorferi* sensu lato (OR = 1.51, 95% Wald CI 1.04–2.19; LRT P = 0.0440) was not valid after adjusting for five tests using the BH method (BH P = 0.0734). No pathogen had a BH-supported component within-site.

The two previously supported total associations were geographically concentrated. For *E. ewingii*, UKFS (University of Kansas Field Station) contributed 111 of 132 matched positives (84.1%), while Treehaven (TREE) contributed 38 of 61 matched *A. phagocytophilum* positives (62.3%). Leave-one-site-out refits did not change the direction of either association (Fig. 6). After excluding UKFS, the *E. ewingii* estimate remained positive (OR = 2.73, 95% CI 0.51–14.44), but the likelihood-ratio P-value was not estimable because precision deteriorated substantially. After excluding TREE, the *A. phagocytophilum* estimate also remained positive but was not supported (OR = 1.36, 95% CI 0.83–2.25; *P = 0.228*). These patterns indicate geographically clustered co-occurrence rather than broadly replicated within-site temporal coupling. The final within-/between-site models had acceptable residual diagnostics. The *E. ewingii* combined quantile test was borderline but nonsignificant (*P = 0.0507*), the *A. phagocytophilum* quantile test was nonsignificant (*P = 0.114*), and the *B. lonestari* model showed a significant quantile departure (*P = 0.00115*), although that outcome had no supported encounter-rate association.

Exploratory testing-coverage and site-influence sensitivity

All 12 exploratory *I. scapularis* binomial sensitivity models converged with positive-definite Hessians, and six reference coefficients were reproduced to numerical precision. The primary encounter association was positive for *A. phagocytophilum* (OR = 1.47 95% CI 1.13–1.90; primary five-test BH P = 0.0218) and was similar in the high-support subset (OR = 1.45 BH P = 0.0403). However, it was attenuated after adding testing fraction (full-data OR = 0.88, 95% CI 0.45–1.74; high-support OR = 1.07, 95% CI 0.51–2.28). Same data coverage-block LRTs were not supported (P = 0.1086 and P = 0.4045). The full-data coverage adjusted model (P = 0.0120) and the jointly decomposed coverage model (P = 0.0164) had deviations, while the high-support coverage model (P = 0.4694) did not (*Supplementary Table S5*) for DHARMa uniformity tests.

For *B. burgdorferi* sensu lato, the primary association was unsupported (OR = 0.92, 95% CI 0.70–1.21; primary five-test BH P = 0.6772), as was the high-support primary estimate (OR = 1.00, 95% CI 0.75–1.32). Further modification of the test-fraction with negative conditional estimates (full-data OR = 0.52, 95% CI 0.32–0.84; high-support OR = 0.45, 95% CI 0.25–0.82) and good within-sample fit (block LRT P = 0.00228 and P = 0.00147). However, when the full data coverage adjusted OR was calculated without the removal of TREE, it was 0.86 (95% CI 0.45–1.64) and the coverage-block LRT P was 0.293. Therefore, the revised, negative estimate was not informative for omitting the dominant contributing site. There were no uniformity, dispersion, and outlier departures detected for the three coverage-sensitive *B. burgdorferi* model specifications analyzed (*Supplementary Table S5*).

There was no association between *A. phagocytophilum* positivity and visit-level catch size in the individual tested ticks (16 informative site-years, 4999 simulations, P = 0.9278). In contrast, a negative association was observed for *B. burgdorferi* sensu lato (33 informative site-years, 9,999 simulations, Z = − 2.974, P = 0.0030). However, exclusion of TREE eliminated this pattern (Z = 0.149, P = 0.8851), as did exclusion of TREE–2019 alone (Z = − 1.208, P = 0.2287). Excluding visits with catches of at least 20 nymphs weakened the negative pattern (P = 0.0326), and excluding both TREE and these large-catch visits eliminated the evidence for an association (P = 0.7439). The score of the TREE was − 33.13, while the network had a score of − 32.02, so the signal was not consistently replicated across sites and was found to be concentrated at one site. These

analyses were preliminary and did not determine the status of infection of the nymphs that were not tested (*Supplementary Table S6*).

Individual-tick pathogen co-detection and species-specific patterns

All 10,382 nymphal *A. americanum* had complete results for the three selected specific pathogens. 262 (2.52%) ticks were positive for one pathogen, 10,119 (97.47%) were negative for all three, and one tick (0.0096%) was positive for two pathogens (*E. chaffeensis* and *E. ewingii*). There was no significant evidence of non-independence of co-detection among the selected *A. americanum* pathogens in any of the three pairwise associations (Fisher or site-stratified). Complete outputs were obtained for the five specific pathogens for all *I. scapularis* nymphs. Of these, 1741 (75.76%) were negative for all the pathogens, 477 (20.76%) were positive for only one of the pathogens, 75 (3.26%) were positive for exactly two and five (0.22%) were positive for exactly three pathogens; thus, 80 (3.48%) were positive for at least two of the five pathogens selected. Passage of BH correction and site stratification of data left four positives pairwise associations unrestricted. *B. burgdorferi* sensu lato co-occurred with *A. phagocytophilum* in 22 ticks (expected under independence = 12.39; Fisher OR = 2.25, 95% CI 1.26–3.92, *BH P = 0.0089*; site-stratified OR = 2.11, 95% CI 1.24–3.60, *BH P = 0.0126*; six informative sites), with *B. microti* in 41 ticks (expected = 15.15; Fisher OR = 5.01, 95% CI 3.08–8.18; *BH P = 2.39 x* 10^{-10}; site-stratified OR = 4.56, 95% CI 2.86–7.27; *BH P = 6.50 x* 10^{-11}) and with *E. muris*-like in 13 ticks (expected = 4.13; Fisher OR = 6.80, 95% CI 2.59–19.03; *BH P = 1.22 x* 10^{-4}; site-stratified OR = 5.97, 95% CI 2.45–14.54; *BH P = 4.13 x* 10^{-5}). *B. microti* and *E. muris*-like were also positively associated (five double-positive ticks; expected = 0.70; Fisher OR = 9.54, 95% CI 2.66–28.25; *BH P = 0.00165*; site-stratified OR = 5.64, 95% CI 1.99–15.97; *BH P = 0.000917*). Only two sites contributed to the latter three site-stratified comparisons, and these were used as exploratory comparisons, even though the statistical signals were strong. No strong correlations were found between any pair of organisms that included *B. miyamotoi*. The most frequent multi-positive *I. scapularis* infections were those with *B. burgdorferi* sensu lato and *B. microti* (36 ticks), *B. burgdorferi* sensu lato and *A. phagocytophilum* (18 ticks), and *B. burgdorferi* sensu lato and *E. muris*-like (12 ticks). Four ticks contained *B. burgdorferi* sensu lato, *A. phagocytophilum*, and *B. microti*; and one tick contained *B. burgdorferi* sensu lato, *B. microti*, and *E. muris*-like. These findings suggest non-random molecular co-detection of several pairs after broad stratification of the sites, but do not imply biological interaction, confirmed within-tick co-infections, nor explicitly consider residual clustering within ticks of the same sampling event. The associations with the less common pathogens were informed by few informative sites and can only be considered exploratory.

Discussion

Standardized, multi-year NEON observations were used to account for a number of processes that are often conflated in tick surveillance: detection of the focal tick, whether any ticks were encountered, how many ticks were collected when they were encountered, how these processes changed seasonally and with recent weather, and whether the intensity of encounter of nymphal ticks correlated to pathogen prevalence. Seasonality was high for all four focus responses to ticks; while occurrence/detection of *A. americanum* was strongly related to recent temperature, abundance of *A. americanum* was not strongly related to recent temperature conditional on detection; and there were significant unexplained differences among plots, events

and sites. Pathogen prevalence also displayed strong spatial structure; Integrated analyses suggested that the strongest relationships between nymph encounter intensity and pathogen prevalence were among sites, rather than in year-to-year relationships within sites. The network was designed to enable continental-scale analyses of ticks, standardized tick counts, and environmental measurements combined with pathogen testing, thus this type of separation is particularly appropriate for the NEON design (Paull et al. 2022).

Seasonal trend of *A. americanum* modeled fairly well matches field observations in north-central Oklahoma that favored adults during the spring and nymphs during the summer (McClung et al. 2023). These results do not indicate a truly biological peak date, but rather a general activity season spanning from late spring to early summer, and a change in the peak date from year to year and site to site in the NEON data indicates that a single calendar date should not be used as a general phenological optimum. There was also statistically significant seasonality for adult *D. variabilis*; however, the amplitude of the modeled seasonality was small compared with the other focal responses. The relatively low modeled seasonality of adult *D. variabilis* may partially reflect variation in activity at different locations with different activity seasons and overlapping adult cohorts as observed with spring and summer cohort activity in Kentucky (Burg 2001). The shallow seasonal curve in the current analysis may thus be due to a mix of sites with varying cohort structure and timing. The most intense and pronounced seasonal trend was recorded for nymphal *I. scapularis*, where the abundance of the species depends on detection and increases during late spring and early summer. This is similar to the overall U.S. synthesis of the phenology of nymphal *I. scapularis* (Eisen 2025). The NEON-wide curve shows one characteristic aspect of the phenology of blacklegged ticks and smooths over significant regional variation in when nymphs emerge, how long they are active, and when activity diminishes.

The most prominent short term weather indicator was a positive relationship between 7-day temperature deviation and adult and nymphal occurrence/detection of *A. americanum*. No positive-abundance weather blocks remained with BH correction, although there was a nominal association for the nymphal *I. scapularis*. This difference is biologically tenable as short-term weather conditions, especially temperature and humidity, have the potential of affecting tick questing behavior and discernibility in sampling (Vail and Smith 1998; Schulze et al. 2001). As a result, the associations between the environment and the likelihood of finding at least one tick might not be the same as the associations between the environment and the count of ticks found given detection (Fletcher et al. 2005). Field observations in New Jersey also revealed strong correlation between ambient meteorological conditions and questing by *A. americanum*; and adults were more frequently collected during warmer parts of the day, but not when temperatures fell < 4.4°C (Schulze et al. 2001). At the NEON-network scale these observational associations are consistent with a higher association between recent warmth and encounter probability than in abundance given an encounter. Lack of a strong weather block in the positive-abundance models should not be taken as an indication that temperature, atmospheric moisture, or precipitation are not relevant to tick ecology (Angell et al. 2026). The relationship between temperature and moisture to the presence and abundance of ticks varies by species, life stage, and region; for example, climate–abundance comparisons were made that showed different relationships between temperature, moisture, and abundance of *A. americanum*, *D. variabilis*, and *I. scapularis* in the state of Illinois (Bacon et al. 2022). Our study demonstrates this context dependence as the same standardized deviations in weather did not account for positive abundance across four focal responses.

Year effects for positive abundance were dependent on the method of estimation of uncertainty. The primary hierarchical models had 11/20 Wald tests that were significant after Benjamini–Hochberg adjustment, and the Wald-significant 2021 and 2024 nymphal *A. americanum* contrasts had site-bootstrap intervals that contained 1, while the site-cluster bootstrap sensitivity intervals contained 1 for adult *D. variabilis* in 2020 and nymphal *I. scapularis* in 2022. The nymphal *A. americanum* ratio in 2021 was above 1 in all 13 leave-one-site-out fits, but with a bootstrap interval that included unity. The full 550-record model was the main analysis for adult *A. americanum* and is not presented as an interval for the unchanged 550-record estimate, because the bootstrap sensitivity cohort excluded the five positive flag-method visits from UKFS and therefore contained 545 of the original 550 positive visits. Seven unadjusted bootstrap percentile intervals did not contain unity in 20 contrasts, two of which were in that restricted cohort; there were no 7 multiplicity-adjusted discoveries. The interannual differences are best viewed as associations between a site and a year and not as network-wide temporal changes as there are only 13–22 sites per group and support of a site varies from year to year.

Random-effect estimates showed that there was a high heterogeneity within the model structures retained but are not meant to measure what proportion of the total variation is explained by weather and/or seasonality. The retained proportion of the random-intercept variance was greater at the plot level than at the event level for all four occurrence/detection models (82.3%, 79.1%, 55.9%, and 57.0% of the total of the random-intercept variance retained for each model, respectively). Variance (plot level versus site level) was slightly greater for abundance conditional on detection for adult *A. americanum*, nymphal *A. americanum* and adult *D. variabilis*, and dominated by site-level variance for nymphal *I. scapularis* (76.6% at the site level versus 23.4% at the plot level). A previous NEON study conducted in Florida highlighted the need to consider spatial and temporal differences and explicitly include imperfect detection, when making abundance estimates (Klarenberg and Wisely 2019). Our models use observed occurrence/detection to make inferences about positive abundance rather than assuming the estimation of latent occupancy or detection probability. These findings suggest that maintaining the hierarchical structure of repeated survey sampling over the continent is advantageous over repeated collections considered as independent observations (Popovic et al. 2024). Residual spatial analyses was another precaution. There was no residual spatial autocorrelation in most final models, although global Moran tests revealed some residual spatial structure in the models for the occurrence of nymphs of *A. americanum* and *I. scapularis*. Multiple-testing correction did not produce a possible distance scale after targeted tests and adding an explicit spatial covariance structure did not produce a valid estimable model for nymphal *A. americanum*, nor did it help to improve the fit of the model for nymphal *I. scapularis*. The prespecified nonspatial hierarchical models were retained, as the spatial sensitivity model for nymphal *A. americanum* had a non-positive-definite Hessian, and incorporating spatial covariance did not improve model fit for nymphal *I. scapularis*. This was then recognized as residual spatial autocorrelation as a limitation of inference (*Supplementary Fig. S1*). There is, however, a residual spatial dependence that should be understood as evidence that some other geospatially structured determinant (e.g., host community, vegetation, microclimate, other habitat attribute) was not represented by the predictors selected (Miller et al. 2007).

Prevalence of the three main pathogens in nymphal *A. americanum* was low; prevalence of *B. lonestari* and *E. chaffeensis* were ~ 0.6% (2019–2024), and *E. ewingii* was 1.3%. These pooled NEON-site estimates are lower than some geographically specific reports, but caution should be exercised when making comparisons as there are many differences between the local studies with respect to life stage, habitat, assay design, and sampling period. For instance, pooled nymphal *A. americanum* from a Missouri study had minimal infection

prevalence of about 1.7% for *E. chaffeensis* and 0.6% for *E. ewingii*, whereas infection prevalence in the adults was significantly higher (Steiert and Gilfoy 2002). The variations between the pooled NEON estimates and the prevalence estimates from Missouri highlight the need to be cautious when extrapolating the prevalence estimates of *Ehrlichia* from any local population to other geographic ranges of *A. americanum*. On the other hand, the hierarchy of *I. scapularis* pathogens was different. *Borrelia burgdorferi* sensu lato was by far the most frequently detected primary pathogen, while *A. phagocytophilum* was detected at a lower observed prevalence. This ordering is similar to national surveillance data, where *B. burgdorferi* sensu stricto is the most common and widely distributed of the species that infect host-seeking *I. scapularis*, and *A. phagocytophilum* is widespread but not as common, and both organisms exhibit significant site-level variation These NEON-wide estimates of 19.7% and 2.7% for *B. burgdorferi* s.l. and *A. phagocytophilum*, respectively, are in a similar general trend to the well-established pattern of high spatial heterogeneity observed in active surveillance programs (Foster et al., 2023).

Temporal prevalence patterns were much less distinct than seasonal patterns in tick abundance. Only *E. ewingii* had strong interannual variation following the final beta-binomial analysis, with adjusted prevalence the highest in 2023, and specifically higher than in 2021 and 2024. The present models do not indicate any temporal trends for *B. burgdorferi* s.l. or *A. phagocytophilum*. The same is true for long-term surveys of *I. scapularis* infection prevalence in the Upper Midwest, where infection prevalence varies highly from year to year at individual sites but shows no consistent year-to-year trends at the regional level, so that infection prevalence is better used to describe coarse acarological patterns than to set fixed annual risk thresholds (Foster et al. 2022). One of the most informative distinctions in this study is the integrated analyses. Initial models suggested positive relationships between nymph encounter rate and prevalence for *E. ewingii* in *A. americanum* and *A. phagocytophilum* in *I. scapularis*. However, when the rate of encounters was expressed as within site and between site contributions it was evident that the signals were mostly between sites. In the case of *E. ewingii*, there was a significant positive relationship between average rates of *A. americanum* nymph encounter and prevalence, but no multiple-testing-corrected relationship between year-to-year differences from a site's own average rate of *A. americanum* encounter with prevalence. A weaker between-site pattern was observed with *A. phagocytophilum* prevalence in *I. scapularis* nymphs. Additionally, this spatial interpretation is especially applicable given an independent analysis of NEON data indicating environmental differentiation between *E. ewingii* and *A. americanum* based on vapor pressure and minimum temperature in which several other vector–pathogen combinations exhibited less or different niche differentiation (Alkishe et al., 2024). In combination, these studies suggest that the distribution of pathogens is also geographically variable within vector distribution. In the recent eight-year NEON study, (Maza et al. 2026) examined spatial synchrony and lagged climate associations for *A. americanum* nymphs, but the current study distinguished between occurrence and conditional abundance and examined visit-matched pathogen results and within- versus between-site associations.

Notably, there was no strong positive correlation between *I. scapularis* nymph abundance and prevalence of *B. burgdorferi*. While a Minnesota survey found that the prevalence of nymphs seeking hosts was not homogenous across space (Johnson et al. 2018), it did not determine the interannual relationship between within-site encounter–prevalence of nymphs, and infected-nymph density. This allows the intensity of vector encounter and prevalence of infection to be considered as two components of the acarological hazard and to be treated separately. The encounter index between infected and non-infected nymphs was taken to be a

descriptive index of prevalence instead of a demonstration of an overall abundance-prevalence relationship. Leave-one-site-out analyses revealed that UKFS and TREE played a significant role in determining the associations between E. *ewingii* and *A. phagocytophilum*, respectively. Omitting these sites-maintained effect directions but at the cost of decreased precision and statistical support. The results indicate that there is no uniform ecological relationship across the entire network but site-dependent associations, which is consistent with prior studies that have shown that *E. ewingii* and *A. phagocytophilum* are geographically heterogeneous in their distribution (Mixson et al. 2006; Foster et al. 2022). Individual-tick analyses indicated that there was rare co-detection of the three selected *A. americanum* pathogens, but 3.48% of complete-panel *I. scapularis* nymphs were molecularly co-detected with two or more pathogens. The *B. microti* associations were not well supported geographically and the positive association between *B. burgdorferi* s.l. and *A. phagocytophilum* was the most supported. These discovery in exploratory research are generally in line with past multi-region surveillance studies of the U.S (Lehane et al. 2021). The agreement is biologically possible because the same organisms are shared by *I. scapularis* and the organisms are found in the same reservoir community (Stewart and Bloom 2020b); however, our handling is intentionally restricted to molecularly co-detected organisms and not necessarily by direct organism interaction, by simultaneous transmission, or of a clinical relevance in coinfection. There are several factors that limit the inferences that can be made. NEON drag/flag sampling is not a measure of actual tick density, and Daymet is not a measure of tick microclimate. Pathogen prevalence was estimated from tested nymphs; exact-visit reconciliation and sensitivity analyses characterized the robustness and remaining limitations of those associations. Not all pathogen signals were geographically uniform and there was a limitation in generalization. Finally, the observational design is not conducive to attributing causality (Springer et al. 2016). The analyses demonstrate the importance of considering tick-borne hazard as a series of interrelated but discrete processes. Tick presence was highly seasonal, and weather had a stronger association with *A. americanum* presence than abundance conditional on finding, although there remained a high level of spatial heterogeneity. There was further spatial structure in pathogen prevalence, and the positive relationship between *A. americanum* encounters and *E. ewingii* prevalence was mostly between-site differences. The most selected pathogen, *B. burgdorferi* sensu lato, was most detected among *I. scapularis* nymphs, and multi-pathogen co-detection was only seen in 3.48% of complete-panel nymphs. Precise-match auditing disclosed that almost all nymph-positive visits had one less tested than collected nymph, and a single-nymph visit had no observations of pathogen-testing. The coverage of testing was thus structurally connected to the size of the catch and could not stand alone to correct selection bias. Even though coverage adjustment led to a better fit of the *B. burgdorferi* model, with a negative coefficient of encounter, this relationship was highly affected by TREE, especially in 2019. The results therefore confirm individual monitoring of tick occurrence, conditional abundance, prevalence of the pathogen, and co-detection but not a general inverse abundance-prevalence relationship and the infection status of untested nymphs. Even though NEON offers standardized longitudinal surveillance, its locations were not nationally representative, and there were geographic and temporal coverage differences between tick species and pathogens. Some inferences on abundance were not made due to residual spatial and temporal dependence and site-cluster bootstrap uncertainty. Drag and flag sampling quantified observed encounters, as opposed to actual occupancy or absolute abundance. The study of pathogen prevalence was only done on nymphs and might have been biased by nonrandom sampling; 262 single-nymphs visits gave no matched pathogen assays, and 110 tested nymphs could not be associated with valid ecological visits. The generalizability was further restricted by geographic concentration of positive *E. ewingii* and *A. phagocytophilum* at UKFS and TREE respectively. Causal

inference was not possible due to unmeasured microclimatic change and the observational design. Lastly, the infected-nymph encounter index is a descriptive proxy and not the actual infected-tick density or risk of human disease and molecular co-detection is not used to determine biological interactions and transmission.

Conclusion

A tick standardized NEON count indicated that there were significant seasonal and spatial trends in the detection, presence, and pathogen prevalence of ticks. The short-term temperature anomalies were correlated with the presence of *A. america*num, whereas the weather-block evidence of positive abundance was not confirmed after the multiple-testing correction. Positive-count seasonality was confirmed for all four species–stage groups, though annual contrasts based on the primary model were sometimes unreliable due to resampling at the site. In the case of pathogen outcome, the encounter–prevalence association between *E. ewingii* and between *A. phagocytophilum* was largely due to between-site differences and were influenced by pathogen-testing coverage and site influence, respectively. Multi-pathogen molecular co-detection was less frequently found in nymphal *A. americanum* and more frequently found in the selected targets in nymphal *I. scapularis*. The infected-nymph encounter index is a descriptive product of the encounter rate and the measured infected-nymph prevalence but cannot be interpreted as an estimate of absolute density of infected-nymphs or human infection risk. Inferences cannot be drawn-out uncritically to unsampled sites or untested ticks because visits were systematically excluded for nearly all single-nymph visits. Surveillance understanding should maintain independent data on detections, effort standardized encounters, pathogen prevalence, spatial heterogeneity and assay coverage.

Declarations

Availability of Data and Materials: All data is available and can be requested from corresponding author on reasonable request.

Funding Support: No specific grants from government, private, or nonprofit funding organizations were obtained for this study.

Conflict of Interest: The authors declare that none of the work reported in this paper was impacted by any known competing financial interests or personal relationships.

Declaration of Generative Artificial Intelligence (AI): Codex was used for statistical and coding purposes and authors take full responsibility for integrity of data.

Author Contributions: MH contributed to design, conceptualization, validation, data curation, methodology, formal analysis and original draft. SA contributed to data curation, and formal analysis. BC contributed to validation, methodology, supervision, critically reviewed and edited manuscript. All authors agreed to the final draft.

References

1. Alkishe A, Cobos ME, Peterson AT (2024) Broad-scale ecological niches of pathogens vectored by the ticks *Ixodes scapularis* and *Amblyomma americanum* in North America. PeerJ 12:e17944. https://doi.org/10.7717/peerj.17944
2. Angell KE, Jarnefeld J, Schiffman EK, et al (2026) Climate and other environmental factors predict tick abundance and Lyme cases in Minnesota one and two years in advance. One Health 23:101507. https://doi.org/10.1016/j.onehlt.2026.101507
3. Bacon EA, Kopsco H, Gronemeyer P, et al (2022) Effects of Climate on the Variation in Abundance of Three Tick Species in Illinois. J Med Entomol 59:700–709. https://doi.org/10.1093/jme/tjab189
4. Benjamini Y, Hochberg Y (1995) Controlling the False Discovery Rate: A Practical and Powerful Approach to Multiple Testing. J R Stat Soc Ser B Stat Methodol 57:289–300. https://doi.org/10.1111/j.2517-6161.1995.tb02031.x
5. Brooks M E, Kristensen K, Benthem K J ,van, et al (2017) glmmTMB Balances Speed and Flexibility Among Packages for Zero-inflated Generalized Linear Mixed Modeling. R J 9:378. https://doi.org/10.32614/RJ-2017-066
6. Brunner JL, LaDeau SL, Killilea M, et al (2023) Off-host survival of blacklegged ticks in eastern North America: A multistage, multiyear, multisite study. Ecol Monogr 93:e1572. https://doi.org/10.1002/ecm.1572
7. Burg JG (2001) Seasonal activity and spatial distribution of host-seeking adults of the tick *Dermacentor variabilis*. Med Vet Entomol 15:413–421. https://doi.org/10.1046/j.0269-283x.2001.00329.x
8. Burtis JC, Bjork J, Johnson TL, et al (2023) Seasonal activity patterns of host-seeking Ixodes scapularis (Acari: Ixodidae) in Minnesota, 2015–2017. J Med Entomol 60:769–777. https://doi.org/10.1093/jme/tjad048
9. Carbone G, Boiardi G, Infantino C, et al (2025) Vectors on the Move: How Climate Change Fuels the Spread of Arboviruses in Europe. Microorganisms 13:2034. https://doi.org/10.3390/microorganisms13092034
10. Childs JE, Paddock CD (2003) The ascendancy of Amblyomma americanum as a vector of pathogens affecting humans in the United States. Annu Rev Entomol 48:307–337
11. Eisen L (2025) Seasonal activity patterns of Ixodes scapularis and Ixodes pacificus in the United States. Ticks Tick-Borne Dis 16:102433. https://doi.org/10.1016/j.ttbdis.2024.102433
12. Eisen RJ, Eisen L (2018) The Blacklegged Tick, Ixodes scapularis: An Increasing Public Health Concern. Trends Parasitol 34:295–309. https://doi.org/10.1016/j.pt.2017.12.006
13. Eisen RJ, Eisen L (2024) Evaluation of the association between climate warming and the spread and proliferation of Ixodes scapularis in northern states in the Eastern United States. Ticks Tick-Borne Dis 15:102286. https://doi.org/10.1016/j.ttbdis.2023.102286
14. Eisen RJ, Paddock CD (2021) Tick and Tickborne Pathogen Surveillance as a Public Health Tool in the United States. J Med Entomol 58:1490–1502. https://doi.org/10.1093/jme/tjaa087
15. Fletcher D, MacKenzie D, Villouta E (2005) Modelling skewed data with many zeros: A simple approach combining ordinary and logistic regression. Environ Ecol Stat 12:45–54. https://doi.org/10.1007/s10651-005-6817-1
16. Foster E, Burtis J, Sidge JL, et al (2022) Inter-annual variation in prevalence of Borrelia burgdorferi sensu stricto and Anaplasma phagocytophilum in host-seeking Ixodes scapularis (Acari: Ixodidae) at long-term

surveillance sites in the upper midwestern United States: Implications for public health practice. Ticks Tick-Borne Dis 13:101886. https://doi.org/10.1016/j.ttbdis.2021.101886

17. Foster E, Maes SA, Holcomb KM, Eisen RJ (2023) Prevalence of five human pathogens in host-seeking Ixodes scapularis and Ixodes pacificus by region, state, and county in the contiguous United States generated through national tick surveillance. Ticks Tick-Borne Dis 14:102250. https://doi.org/10.1016/j.ttbdis.2023.102250
18. Hahn MB, Bjork JKH, Neitzel DF, et al (2018) Evaluating acarological risk for exposure to Ixodes scapularis and Ixodes scapularis-borne pathogens in recreational and residential settings in Washington County, Minnesota. Ticks Tick-Borne Dis 9:340–348. https://doi.org/10.1016/j.ttbdis.2017.11.010
19. Hartig F (2016) DHARMa: residual diagnostics for hierarchical (multi-level/mixed) regression models. CRAN Contrib Packag
20. Johnson TL, Graham CB, Maes SE, et al (2018) Prevalence and distribution of seven human pathogens in host-seeking Ixodes scapularis (Acari: Ixodidae) nymphs in Minnesota, USA. Ticks Tick-Borne Dis 9:1499–1507. https://doi.org/10.1016/j.ttbdis.2018.07.009
21. Kache PA, Bron GM, Zapata-Ramirez S, et al (2023) Evaluating spatial and temporal patterns of tick exposure in the United States using community science data submitted through a smartphone application. Ticks Tick-Borne Dis 14:102163. https://doi.org/10.1016/j.ttbdis.2023.102163
22. Klarenberg G, Wisely SM (2019) Evaluation of NEON Data to Model Spatio-Temporal Tick Dynamics in Florida. Insects 10:321. https://doi.org/10.3390/insects10100321
23. Lehane A, Maes SE, Graham CB, et al (2021) Prevalence of single and coinfections of human pathogens in Ixodes ticks from five geographical regions in the United States, 2013–2019. Ticks Tick-Borne Dis 12:101637. https://doi.org/10.1016/j.ttbdis.2020.101637
24. Lenth R (2023) emmeans: Estimated Marginal Means, aka Least-Squares Means_. R Package Version 18 5
25. Martin TG, Wintle BA, Rhodes JR, et al (2005) Zero tolerance ecology: improving ecological inference by modelling the source of zero observations. Ecol Lett 8:1235–1246. https://doi.org/10.1111/j.1461-0248.2005.00826.x
26. Maza SR, Barton JH, Zuckerberg B, et al (2026) Spatiotemporal dynamics of *Amblyomma americanum* abundance and infection prevalence across a subcontinental scale. Ecosphere 17:e70797. https://doi.org/10.1002/ecs2.70797
27. McClung KL, Sundstrom KD, Lineberry MW, et al (2023) Seasonality of Amblyomma americanum (Acari: Ixodidae) Activity and Prevalence of Infection with Tick-Borne Disease Agents in North Central Oklahoma. Vector-Borne Zoonotic Dis 23:561–567. https://doi.org/10.1089/vbz.2023.0009
28. McClure M, Diuk-Wasser MA (2019) Climate impacts on blacklegged tick host-seeking behavior. Int J Parasitol 49:37–47. https://doi.org/10.1016/j.ijpara.2018.08.005
29. Miller J, Franklin J, Aspinall R (2007) Incorporating spatial dependence in predictive vegetation models. Ecol Model 202:225–242. https://doi.org/10.1016/j.ecolmodel.2006.12.012
30. Mixson TR, Campbell SR, Gill JS, et al (2006) Prevalence of *Ehrlichia*, *Borrelia*, and *Rickettsial* Agents in *Amblyomma americanum* (Acari: Ixodidae) Collected from Nine States. J Med Entomol 43:1261–1268. https://doi.org/10.1093/jmedent/43.6.1261

31. Moran PA (1950) A test for the serial independence of residuals. Biometrika 37:178–181
32. Ogden NH, Ben Beard C, Ginsberg HS, Tsao JI (2021) Possible Effects of Climate Change on Ixodid Ticks and the Pathogens They Transmit: Predictions and Observations. J Med Entomol 58:1536–1545. https://doi.org/10.1093/jme/tjaa220
33. Paull S (2026) NEON User Guide to Ticks Sampled Using Drag Cloths (DP1.10093.001) and Tick-borne Pathogen Status (DP1.10092.001). National Ecological Observatory Network (NEON), Battelle, Boulder, Colorado, USA.
34. Paull SH, Thibault KM, Benson AL (2022) Tick abundance, diversity and pathogen data collected by the National Ecological Observatory Network. Gigabyte 2022:1–11. https://doi.org/10.46471/gigabyte.56
35. Pepin KM, Eisen RJ, Mead PS, et al (2012) Geographic Variation in the Relationship between Human Lyme Disease Incidence and Density of Infected Host-Seeking Ixodes scapularis Nymphs in the Eastern United States. Am Soc Trop Med Hyg 86:1062–1071. https://doi.org/10.4269/ajtmh.2012.11-0630
36. Popovic G, Mason TJ, Drobniak SM, et al (2024) Four principles for improved statistical ecology. Methods Ecol Evol 15:266–281. https://doi.org/10.1111/2041-210X.14270
37. Randolph SE (2004) Tick ecology: processes and patterns behind the epidemiological risk posed by ixodid ticks as vectors. Parasitology 129:S37–S65. https://doi.org/10.1017/S0031182004004925
38. Rosenberg R, Lindsey NP, Fischer M, et al (2018) Vital Signs: Trends in Reported Vectorborne Disease Cases — United States and Territories, 2004–2016. MMWR Morb Mortal Wkly Rep 67:496–501. https://doi.org/10.15585/mmwr.mm6717e1
39. Schulze TL, Jordan RA, Hung RW (2001) Effects of Selected Meteorological Factors on Diurnal Questing of Ixodes scapularis and Amblyomma americanum (Acari: Ixodidae). J Med Entomol 38:318–324. https://doi.org/10.1603/0022-2585-38.2.318
40. Sharma Y, Laison EKE, Philippsen T, et al (2024) Models and data used to predict the abundance and distribution of Ixodes scapularis (blacklegged tick) in North America: a scoping review. Lancet Reg Health - Am 32:100706. https://doi.org/10.1016/j.lana.2024.100706
41. Sonenshine D (2018) Range Expansion of Tick Disease Vectors in North America: Implications for Spread of Tick-Borne Disease. Int J Environ Res Public Health 15:478. https://doi.org/10.3390/ijerph15030478
42. Springer YP, Hoekman D, Johnson PTJ, et al (2016) Tick-, mosquito-, and rodent-borne parasite sampling designs for the National Ecological Observatory Network. Ecosphere 7:e01271. https://doi.org/10.1002/ecs2.1271
43. Steiert JG, Gilfoy F (2002) Infection Rates of Amblyomma americanum and Dermacentor variabilis by Ehrlichia chaffeensis and Ehrlichia ewingii in Southwest Missouri. Vector-Borne Zoonotic Dis 2:53–60. https://doi.org/10.1089/153036602321131841
44. Stewart PE, Bloom ME (2020) Sharing the Ride: Ixodes scapularis Symbionts and Their Interactions. Front Cell Infect Microbiol 10:142. https://doi.org/10.3389/fcimb.2020.00142
45. Thornton MM, Shrestha R, Wei Y, et al (2022) DaymetDaymet: Daily Surface Weather Data on a 1-km Grid for North America, Version 4 R1. 0 MB
46. Thornton PE, Shrestha R, Thornton M, et al (2021) Gridded daily weather data for North America with comprehensive uncertainty quantification. Sci Data 8:190. https://doi.org/10.1038/s41597-021-00973-0

47. Vail SG, Smith G (1998) Air Temperature and Relative Humidity Effects on Behavioral Activity of Blacklegged Tick (Acari: Ixodidae) Nymphs in New Jersey. J Med Entomol 35:1025–1028. https://doi.org/10.1093/jmedent/35.6.1025

Figures

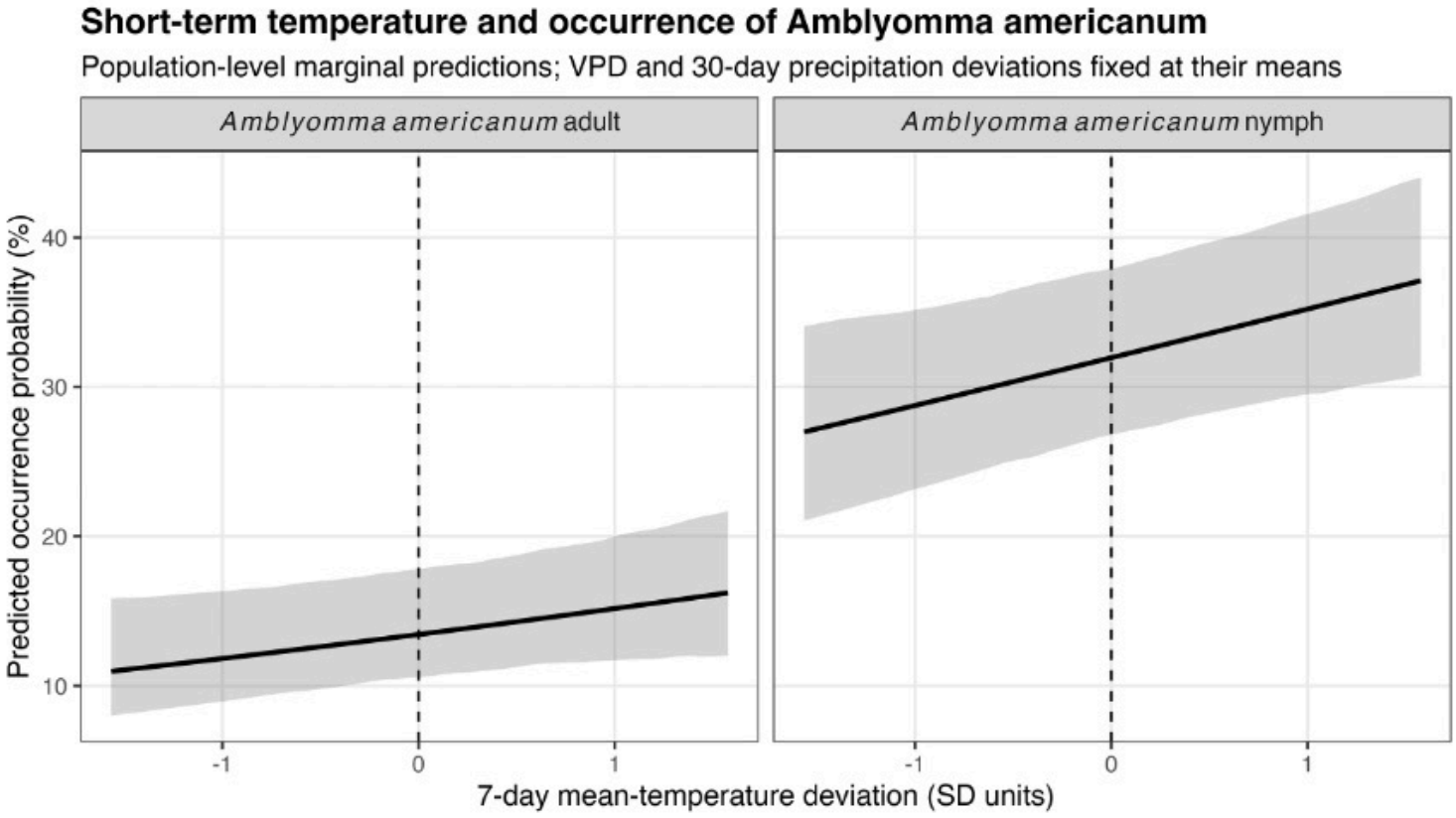

Figure 1

Marginal relationship between standardized 7-day mean-temperature deviation and *A. americanum* occurrence/detection probability. The 30-day precipitation deviations and VPD were kept at their means.

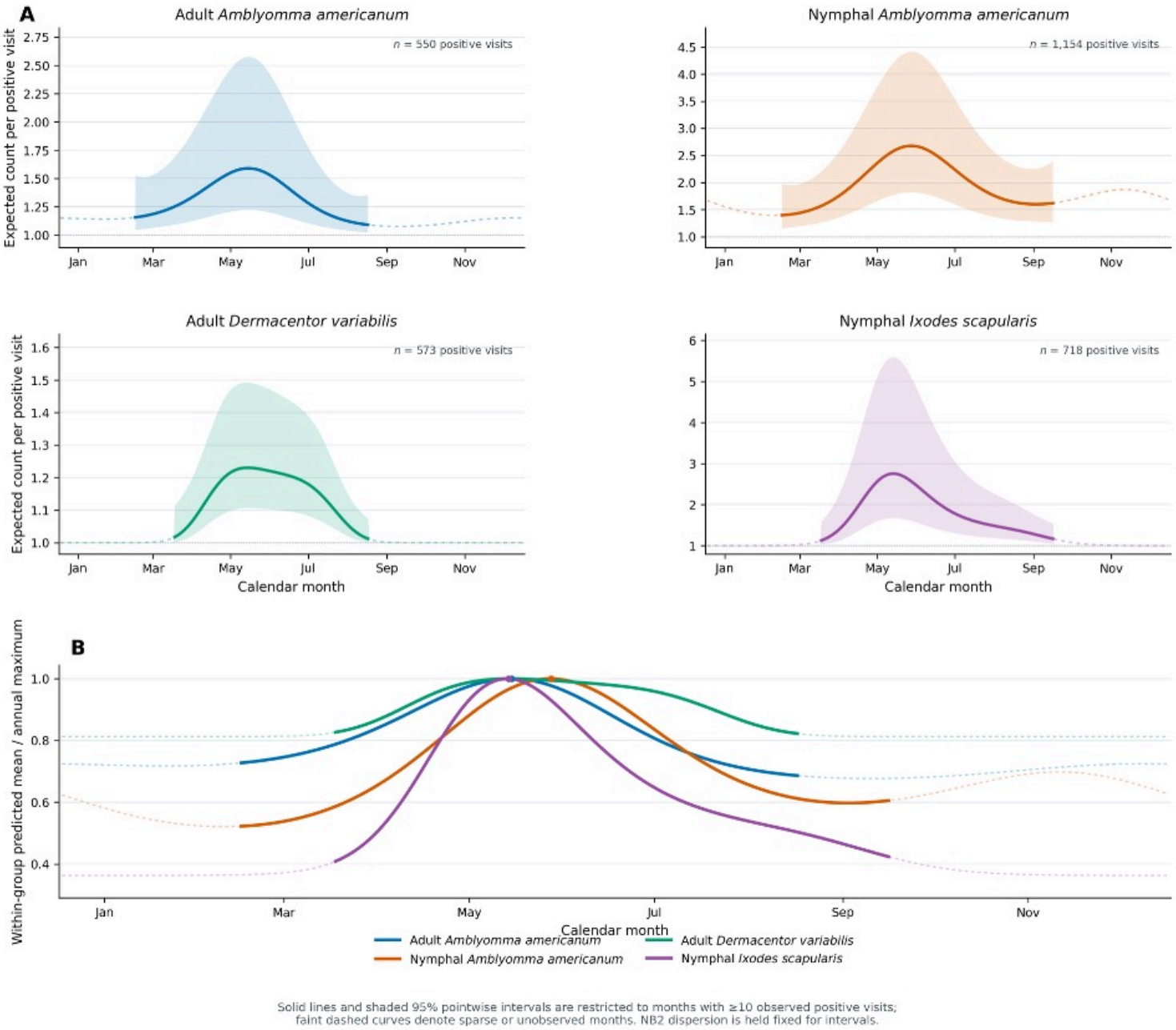

Figure 2

Seasonal abundance based on updated type 2 models, a hierarchical zero-truncated negative-binomial model. (A) The plot and site random intercepts are set to zero, and the expected positive counts following drag sampling for reference year 2019 and the model-specific median sampled area are shown. Solid curves and shaded pointwise 95% Wald confidence intervals are shown only for months where there are at least 10 positive visits (across 2019-2024 years) and faint dashed curves are shown for sparsely sampled or unobserved months. The intervals were computed on the log-link scale, and subsequently back-transformed to the zero-truncated conditional mean, while the fitted NB2 dispersion was fixed. Relative seasonal timing is described as each group's modelled conditional mean divided by the annual maximum for that group (B). Also, the lower boundary is marked with a conditional mean, which restricts the phenological meaning of the relative values, especially for phenological groups with low seasonal amplitude. These intervals are not simultaneous

confidence bands, do not incorporate uncertainty due to the dispersion parameter, and are not prediction bands for individual visits.

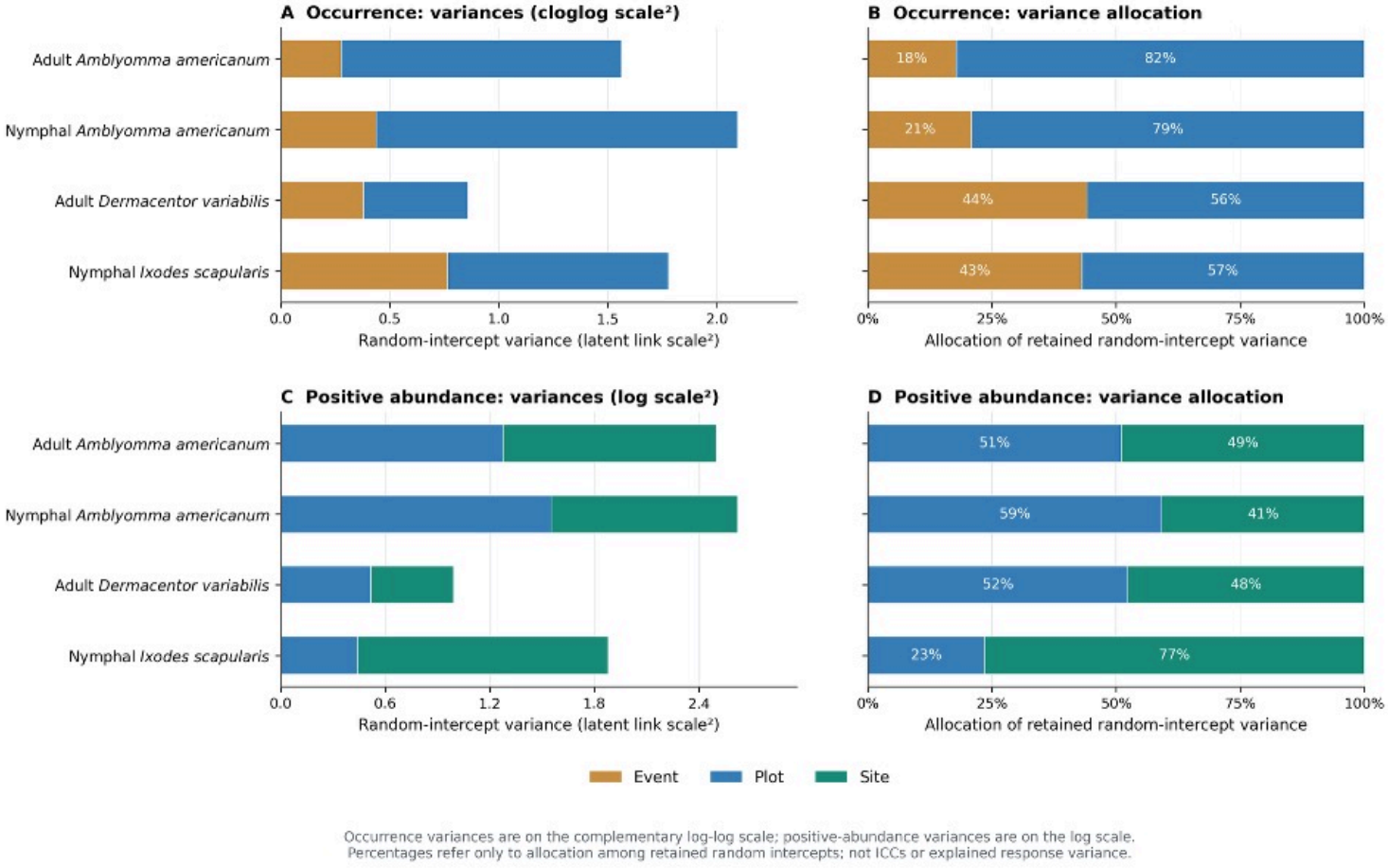

Figure 3

Model selected random-intercept heterogeneity in occurrence/detection and corrected hierarchical positive abundance models. (A) Event- and plot-level random-intercept variances from occurrence models, on the complementary log-log link scale. (B) Distribution of random-intercept variance for occurrence model among retained levels. (C) Plot- and site-level random-intercept variances from revised zero-truncated NB2 positive-abundance models, on the log-link scale. (D) Partitioning of the positive abundance random-intercept variance within retained levels. Occurrence models are based on their chosen baseline/weather specification, while positive-abundance results are based on their revised full seasonal models. The absolute values of the variances are not directly comparable across different scales of links. Shares are not intraclass correlation coefficients nor proportions of the variance of the observed outcome, but simply allocations among retained random-intercept terms.

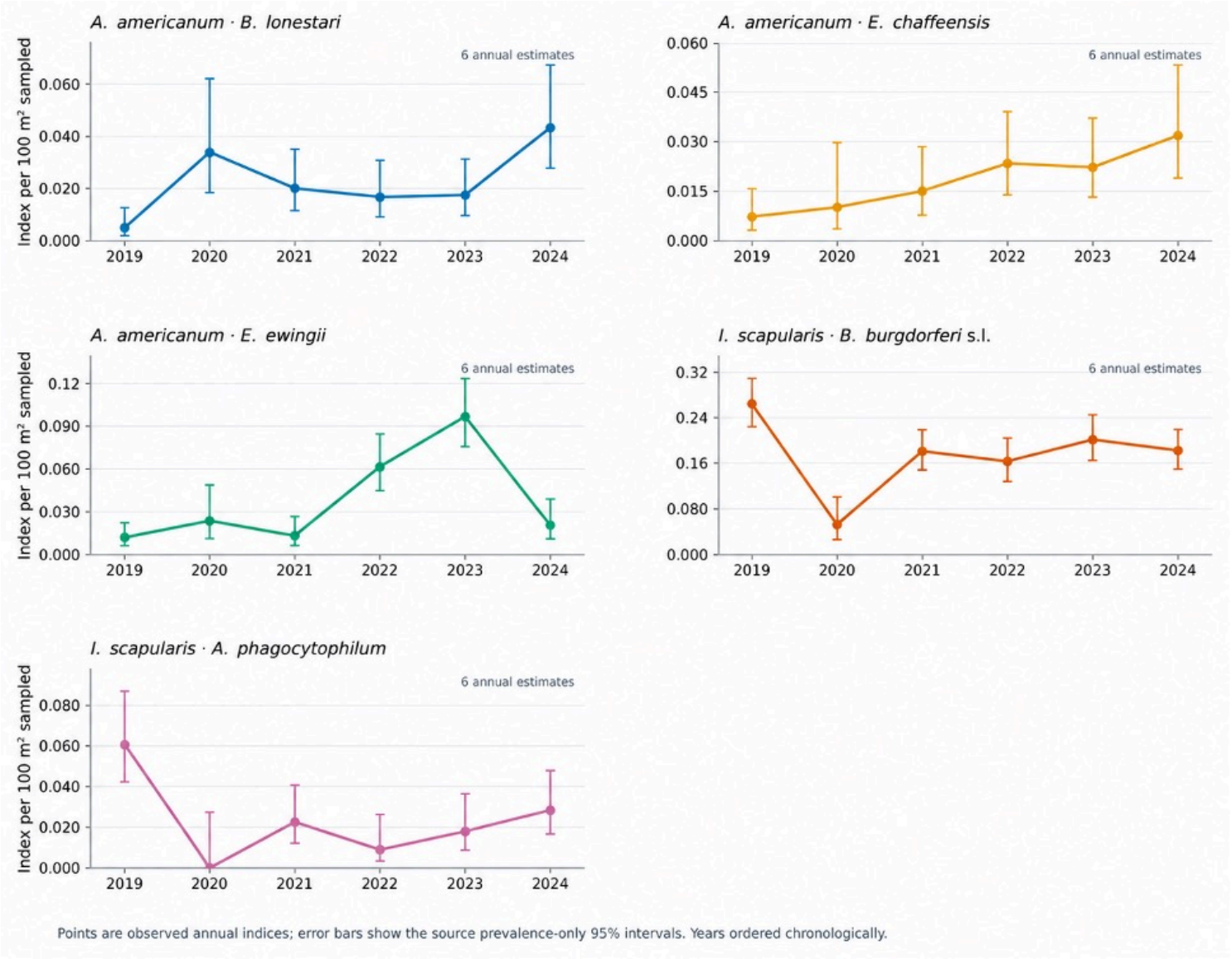

Figure 4

Average number of encounters with infected nymphs per year for the five major vector–pathogen interactions. The index is the number of nymphs encountered per unit effort (100 m²) collected from all eligible visits within pathogen tested site-years and multiplied by the pathogen prevalence sampled in nymphs. Points represent annual encounter-index estimates; error bars are 95% intervals propagating pathogen-prevalence uncertainty only. Uncertainty in encounter rates and nonrandom pathogen-testing selection is not included. The index is not an absolute estimate of infected-nymph density, nor of risk to humans.

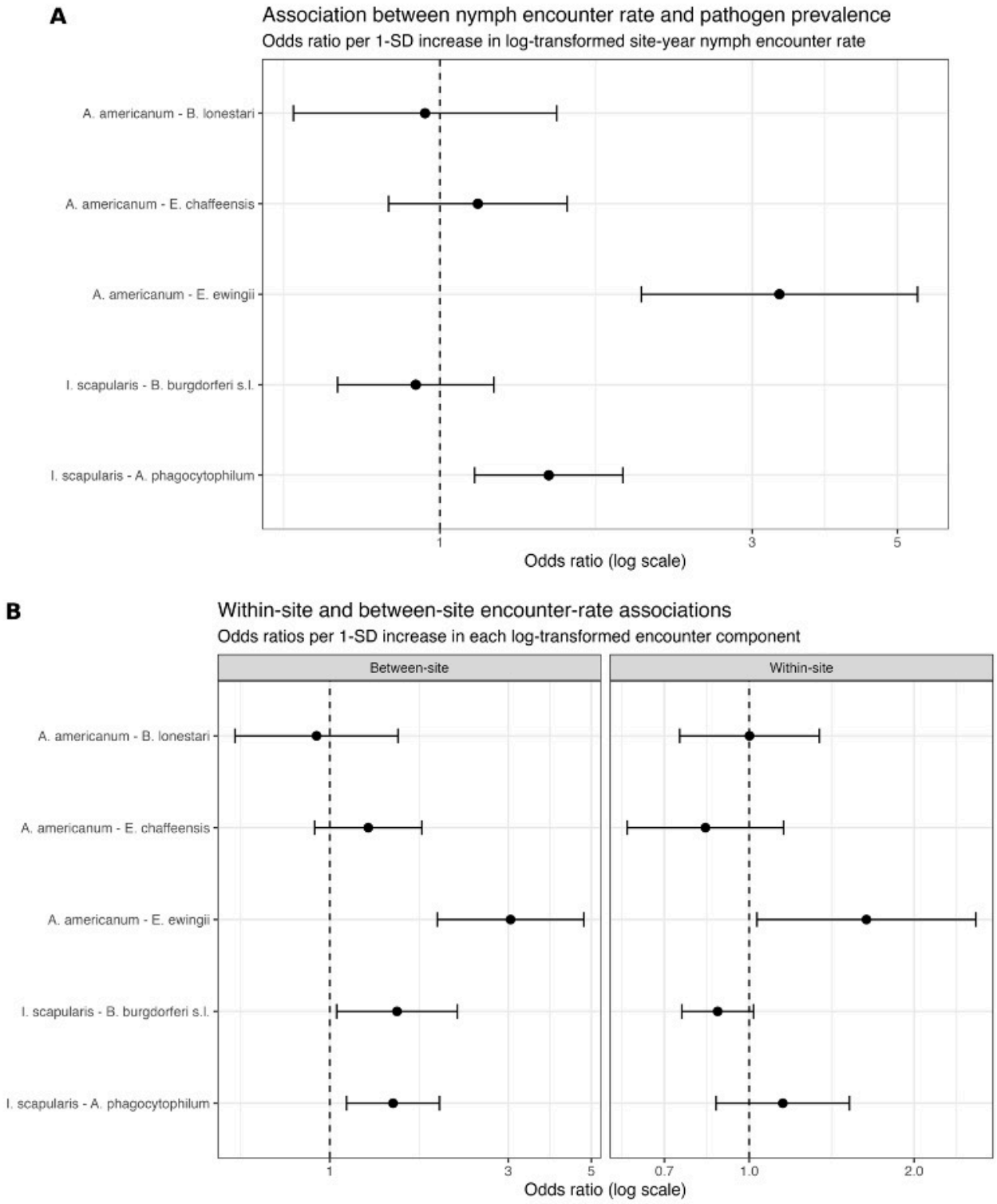

Figure 5

Associations between site-year nymph encounter rate and pathogen prevalence. (A) Total encounter-rate association per 1-SD increase in the log1p-transformed predictor. (B) Between-site (left facet) and within-site (right facet) components, each independently standardized. Points show odds ratios and whiskers are unadjusted 95% Wald confidence intervals. The dashed line indicates OR = 1. Points do not encode BH significance. Family-specific BH-adjusted P values and inferential support are reported in Supplementary Table

S2. In a conservative correction across all ten component tests, only the between-site *E. ewingii* association remained supported (BH P = 0.0240).

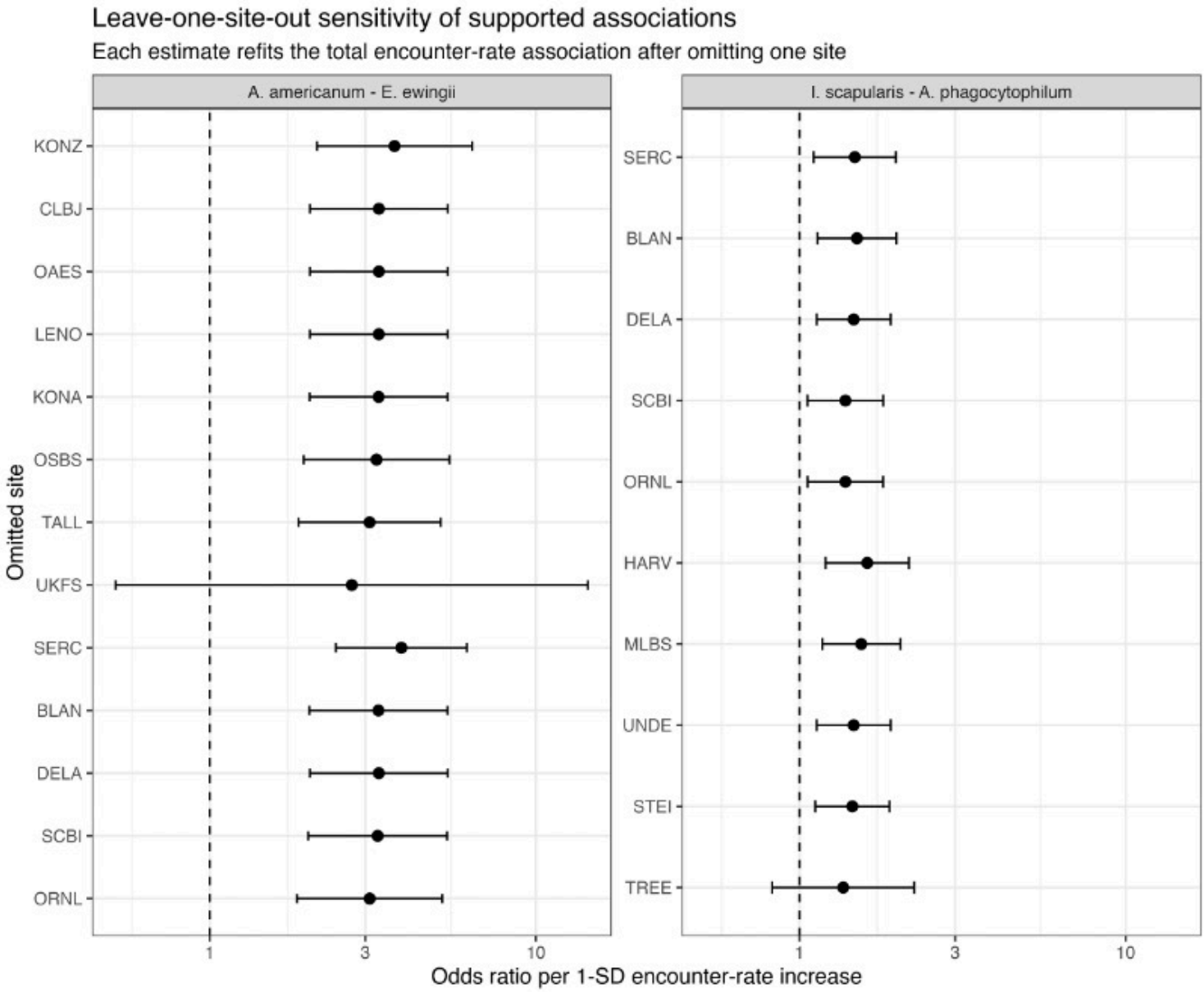

Figure 6

Leave-one-site-out sensitivity for the two pathogen outcomes supported in the primary total encounter-rate analysis. These are total (encounter-rate) associations, after excluding the labeled site, with bars as 95% Wald confidence intervals. The major positive contributor sites for *Ehrlichia ewingii* and *Anaplasma phagocytophilum* were UKFS and TREE, respectively.

Supplementary Files

This is a list of supplementary files associated with this preprint. Click to download.

- SUPPLEMENTARYMATERIALS.docx